POLITECNICO DI MILANO

SCUOLA INTERPOLITECNICA DI DOTTORATO

Doctoral Program in Bioengineering

Final Dissertation

# Advanced human-robot cooperation in neurosurgery

Elisa Beretta

*Supervisors*
prof. Giancarlo Ferrigno
Elena De Momi, PhD

*Co-ordinator of the Research Doctorate Course*
prof. Andrea Aliverti

5th March 2015


POLITECNICO DI MILANO
DEPARTMENT OF ELECTRONICS INFORMATION AND BIOENGINEERING
DOCTORAL PROGRAMME IN BIOENGINEERING

---

# ADVANCED HUMAN-ROBOT COOPERATION IN NEUROSURGERY

Doctoral Dissertation of:
**Elisa Beretta**
784896

Supervisors:
**Elena De Momi, PhD**
**Prof. Giancarlo Ferrigno**

Tutor:
**Pietro Cerveri, PhD**

The Chair of the Doctoral Program:
**Prof. Andrea Aliverti**

2015 – XXVII

# Abstract

Over the last decades, neurosurgery has greatly benefitted from the introduction of image-guided techniques and robotic devices. Thanks to their superior resolution, geometric accuracy and indefatigability, robotic systems are mainly used as an accurate and repeatable tool support system during keyhole procedures. Conversely, open-skull procedures for brain resection/disconnection are traditionally performed free-hand with intraoperative physiological monitoring techniques to identify the functional (eloquent) cortical/subcortical areas, which has to be preserved during the surgery. In particular, direct electrical brain cortex stimulation encompasses the repetitive execution of target reaching gestures on delicate tissue. The conventional approach can benefit from the introduction of a cooperatively controlled robotic assistant, to provide increased positional accuracy and reduce the surgeon's fatigue during the holding phase. Moreover, it could allow the acquisition of the target positions and guide the surgeon towards the recorded sites, thus increasing the reliability of the intraoperative monitoring technique.

In this thesis, we investigated and developed new methodologies for human-robot and robot-tissue interaction control, specifically designed to augment surgeon's skills during cooperatively assisted targeting tasks on soft tissues. Differently from the standard force-to motion control schema, the control approach proposed exploited the high compliance of a redundant flexible joints industrial manipulator. The validation was performed in a realistic setup with brain-mimicking phantoms, enrolling naïve users as well as novice and expert neurosurgeons. The research was focused on these particular research topics:

(*i) investigate the best control strategy for a comfortable and effective cooperation during patient targeting approaching.* The reaching task with the proposed space variable damping controller was shown under laboratory condition to result in reduced targeting error, which guarantees the respect of the position accuracy requirement, and user efforts, which ensure that assisted tool trajectories feel natural to the user.

*(ii) investigate the best control strategy for a safe and stable placement of surgical instruments on soft tissue during the tool placement.* The proposed non-linear force feedback controller was shown to improve the user's skill in performing tool's placement

on brain-mimicking soft tissue, both in terms of contact stability, i.e. reduction of the free-hand tremor by a factor of 10, and contact safety, i.e. 50% reduction of the tissue's indentation.

*(iii) preliminarily study the feasibility of the proposed control approaches for brain cortex stimulation procedures.* The proposed control criteria resulted in comparable performances with respect to state-of-the-art admittance schema with fixed parameters, in terms of pointing accuracy (<1mm) and tissue's indentation overshooting rejection, allowing for the accurate, stable and safe contact with the soft tissue, but at the same time the user efforts during the guidance were reduced by more than 60%.

All the developed controllers were tested in the scope of the EU funded project for brain surgery ACTIVE (FP7-ICT-2009-6-270460). This work support the feasibility of the use of a cooperatively controlled manipulator to assist targeting tasks in open-skull neurosurgery and is in line with the actual research trend in medical robotics, which propose devices that are *effective*, *safe*, both for the patient and the clinical staff in the operating room, and at the same time that provide the surgeon with interfaces as *intuitive* and *familiar* as possible, in order to reduce the training period and facilitate the acceptance of the technology in clinics.

# Acknowledgements

*First of all thanks to my family. Thank you Dad, for pushing me hard and teaching me not to make do with what you have. Thank you Mum, for all your patience and support. Thank you guys, for letting me be your "big sister" even when I was away. Un grazie speciale alla nonna Mary e alla nonna Polly per aver sempre creduto in me.*

*Thanks to the Nearlab group, past and present members. A special thanks to my supervisor Elena for her strong passion and enthusiasm. Without her deadlines, I would probably not be here now. Thank you prof. Ferrigno for the wise advices, the scientific discussions and the "stress tests" of the system during these three years. Thanks to the old generation, colleagues and friends, with whom I have grown up both as an engineer and as a human being. Danilo, you know you are my "light in the dark"! Thank you Alberto, Mirko and Chiara for having shared with me most of this experience (and having taught me how to use Skype!). Thanks to the new generation, for your support, patience and availability. You have been precious collaborators and now I will do my best to pay you back with all the experimental sessions you can possibly want me to participate to!*

*Thanks to prof. Rodriguez y Baena for hosting me in his Lab and to all the MiMlab members, for making my staying in the UK one of the most open-minded period of my academic and personal life.*

*Last, but not least, thanks to my friends from "Brianza": Silvia, Daniela, Elisa, Simona and Daniele. Your have never given up believing in me, even when there were reasons to (you know, " … 110 e lode … 2 volte …"). Thanks to Mattia: I would have starved without your help. You're the best roommate ever! Finally, thanks to Marco: you have accompanied me along the last steps of this journey, the most difficult ones, and you kept your promise. I heartily thank you.*

# Contents

# List of Acronyms

| | |
|---|---|
| ACTIVE | Active Constraints Technologies for Ill-defined or Volatile Environments |
| ADM | ADMittance |
| CAS | Computer Assisted Surgery |
| CRAS | Computer and Robot Assisted Surgery |
| CO | Constant Optimal |
| CT | Computer Tomography |
| DoF | Degree of Freedom |
| EE | End-Effector |
| EOR | Extend of Resection |
| ES | Expert Surgeon |
| FFE | Force Feedback Enhancement |
| FH | Free Hand |
| GC | Gravity Compensation |
| GUI | Graphical User Interface |
| IQR | Inter Quartile Range |
| LWR | Light Weight Robot |
| MRI | Magnetic Resonance Imaging |
| N | Naïve subject |
| NS | Novice Surgeon |
| OROCOS | Open RObot COntrol Software |

| | |
|---|---|
| RA | Robotic Assisted |
| RCM | Remote Centre of Motion |
| RF | Reference Frame |
| ROS | Robot Operating System |
| RMS | Root Mean Square |
| SEEG | StereoElectroEncephaloGraphy |
| SV | Space Variable |
| TCP | Tool Center Point |

# Chapter 1

# Introduction

## 1.1 Computer assisted and robotic neurosurgery

The surgical activity is one of the most challenging tasks performed by humans, which requires complex manual as well as cognitive skills, trained during years of education and practice, together with intuition, passion and ability to manage stress.

Over the last century, medical technologies have entered the operating rooms in order to facilitate the execution of surgical tasks during the intervention. Computer Assisted Surgery (CAS) is a set of methods to assist the surgeon in carrying out the procedure, from the pre-operative planning of the intervention to the post-operative assessment, proving guidance tools to check the correctness of the procedure in the intra-operative phase. In the last decades, Computer and Robot Assisted Surgery (CRAS) extended the concept of CAS, including the use of robotic devices in the surgical environment to behave as active support for the execution of specific tasks, proving greater accuracy and precision (Davies, 2000).

Among all the surgery disciplines, neurosurgery has greatly benefitted from the introduction of image-guided techniques and robotic devices. Neuronavigation systems, such as the Cranial Navigation software (BrainLab, Germany) (Frey et al. 2014) and StealthStation (Medtronic, Minnesota, US)(Gralla et al. 2003), allow the surgeons to plan the intervention on pre-operative MRI-CT patient-specific images and intra-operatively display the position of the tracked surgical tools in relation to the patient data. Thanks to their superior resolution, geometric accuracy and indefatigability, robotic systems are mainly used to aid the surgeon during keyhole neurosurgery.

### 1.1.1 Keyhole neurosurgery

The aim of the keyhole approach is to maximally treat neurosurgical conditions through minimal tissue dissections, reducing tissue trauma and consequent hospitalization time. Encompassing small skull incisions, keyhole neurosurgical procedures are performed by mean of positioning, orienting and advancing the surgical tool to the desired target point in the brain tissue (Dogangil et al. 2010).

In all the cases in which the surgical instrument must be precisely aligned with the pre-operative plan, robots provide an accurate and repeatable alignment tool (Lefranc et al. 2014). The ability of the manipulator to move autonomously to a location along complex 3-dimentional paths and hold the location for long time, rigidly and with-out tremor (Davies, 2000), is the major reason for the development of CRAS in keyhole neurosurgery. Another advantage is that robotic devices can implement remote-center-of-motion (RCM) constraints to decouple the translational and rotational motion of the tool (Taylor and Stoianovici, 2003), e.g. providing the angular mobility required about the entry-point on the skull during neuroendoscopy procedures.

Examples of neurosurgical robotic systems are the Neuromate® system (Renishaw Ltd., UK) (Varma and Eldridge, 2006) (Cardinale et al. 2013), used for deep brain stimulation, stereoelectroencephalography (SEEG) and neuroendoscopy, the ROSA™ system (MedTech, France)(Lefranc et al. 2014), used for neuroendoscopy, SEEG and biopsy, and the CyberKnife (Accuracy Inc, Sunnyvale, CA) (Kuo et al. 2003) (Karam et al. 2014), used for radiosurgery. Recently, the use of needle insertion devices (De Lorenzo, Koseki et al. 2013) and flexible steerable probes (Engh et al. 2010) (Frasson et al. 2010) has been proposed for keyhole neurosurgery.

### 1.1.2 Open-skull neurosurgery

Open-skull neurosurgery encompass a craniotomy, in which a bone flap is temporarily removed from the skull to access the brain, and disconnection and/or resection operations are performed on the exposed brain tissues. Examples of open-skull procedures are the tissues disconnection to expose ruptured middle cerebral artery aneurysm for microsurgical

clipping (Dashti et al. 2007) (Izumo et al. 2014), the tumor removal in glioma surgery (Dziedzic and Bernstein, 2014) and the resection of the epileptogenic zone in drug-resistant epilepsy surgery (Zhang et al. 2013).

In procedures where tissue's resection is performed, e.g. glioma surgery and epilepsy surgery, the extend of the resection (EOR) is a measure of the radicality of the procedure and is correlated to the efficacy of the surgical treatment (Barbosa et al. 2014). Different assistive technologies were proposed in the past decades to improve the EOR, while preserving neurological functions of the brain:

- *Neuronavigation technologies*, which suffer from the lack of consistency between the intra-operative scenario and the pre-operational images due to brain shift (Spena et al. 2013);
- *Intraoperative MRI*, which provides valuable information and real-time feedback for the brain-shift corrections, but it does not provide the precise identification of the tumor margins, particularly critical for resections close to eloquent areas (Barbosa et al. 2014);
- *Intraoperative neurophysiological monitoring*, which is the standard practice in conventional surgery, where an intra-operative mapping is performed in order to identify the functional areas of the brain which has to be preserved. Although extensively used, the reliability of intraoperative neurophysiological monitoring is not optimal (accurate localization of the central sulcus between 91-94% of patients) (Duffau, 2010).

The traditional surgical approach can benefit from the introduction of a robotic assistant during the execution of specific surgical task, where high positional accuracy is required, increasing the clinical outcomes of the procedures and/or reducing the neurosurgeon's execution efforts, especially in maintaining arbitrary stable tool's positions. The NeuroArm® system (IMRIS, Calgary, AB), which is a teleoperated magnetic resonance (MR)-compatible image-guided robot (Sutherland et al. 2008), is the only example of robotic system for open-skull microsurgery. The surgeon is positioned at a remote workstation, guides the motion of the manipulators through hand controllers and uses human-machine interfaces proving MR images and real-time 3-dimentional images of the surgical site. Although the use of intraoperative high-quality imaging allows the surgeon to

partially correct for brain shift, the cost of the system is very high and the interfaces provided in the tele-manipulation scenario are not familiar to the surgeon, requiring a slow learning process in order to acquire confidence and comfort during the operation while accounting for variation of the pathologies (Sutherland et al. 2013).

## 1.2 Intraoperative neurophysiological monitoring

Neurophysiological monitoring (Barbosa et al. 2014) is an intraoperative assistive technique performed in awake craniotomy, during which the surgeon stimulates exposed brain cortical/subcortical areas recording the patient's responses in order to reliably identify

**Figure 1.1** Intraoperative brain mapping of the motor cortex during glioma surgery. The neurosurgeon is performing the stimulation with a monopolar probe (up left) while the electric brain activity (lower) is recorded from superficial electrodes placed on the cortex (up right) in order to detect the occurrence of unwanted stimulation-induced seizures.

'eloquent' cortical areas and subcortical pathways involved in motor, sensory, language and cognitive functions (Figure 1.1).

Performed manually in different phases of the surgical procedure (Spena et al. 2013), direct electrical brain cortex stimulation encompasses the repetitive execution of target reaching gestures, to guarantee a direct control of the functional topography during the tumor removal in glioma surgery (Beez et al. 2013) or of the epileptogenic zone in epilepsy surgery (Zhang et al. 2013). The standard protocol suggests that each site of interest is stimulated at least 3 times non consecutively every $5mm^2$, in order to avoid false-positive and reduce false-negative stimulation results (Szelènyi et al. 2010) (Sanai and Berger, 2010). The duration of the stimulation for brain mapping can vary between 2-4ms (motor functions) and 3-4s (language and cognitive functions). Schematics of the probes used for bipolar or monopolar stimulations (ball tips diameters in the range 2-5mm) are reported in Figure 1.2. In order to visualize the cortical areas involved in motor, cognitive or language functions, sterile tags with numbers or letters are placed on stimulation-sensitive spots (Duffau, 2010) (Figure 1.3).

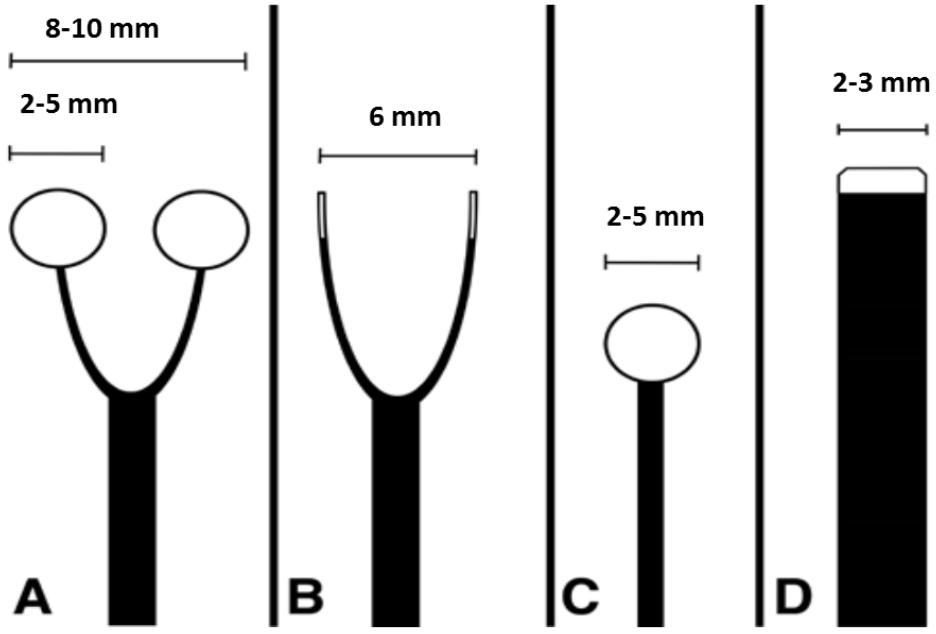


**Figure 1.2** Schematic of probes used for bipolar stimulation with ball tips **(A)** or straight tips **(B)** and for monopolar stimulations with a ball tip **(C)** or straight tip **(D)** [Adapted from Szelènyi et al. 2010]

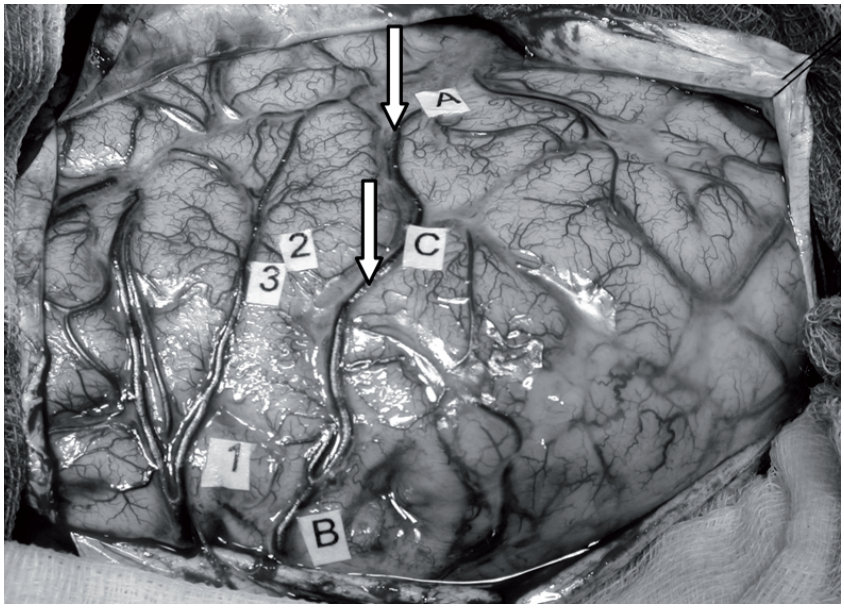


**Figure 1.3** Intraoperative view before glioma resection after electrostimulation mapping, delineated by letter tags. Arrow: precentral sulcus. [Adapted from Duffau, 2010].

### 1.2.1 Brain mapping: clinical requirements

The two main clinical requirements for brain targeting tasks are:

- *pointing accuracy:* the ability of the user to place the tip of the surgical instrument on the intended site and to maintain a stable contact with the underneath tissue.
- *contact safety:* the ability to position the surgical tool in contact with the brain, preserving the integrity of the tissue, thus avoiding damages due to unwanted penetration and reducing interaction forces.

In conventional open-skull neurosurgery, the first requirement is strictly influenced by human *tremor*, which in this context is used to indicate any involuntary hand motion that creates position error (MacLachlan et al. 2012), including physiological tremor and hand drift. Arm support (elbow and/or forearm resting) and a magnification (up to x10) of the visual feedback, e.g. use of a microscope, improve accuracy in task requiring fine manipulation (Safwat et al. 2009). Normal hand tremor under microsurgical conditions is typically several hundred micrometers peak-to-peak (Sandoval et al. 2007), although the maximum deviation from the mean position may reach values up to 2.2mm during a

stationary task, i.e. holding motionless a closed scissor for 5s. During brain cortex stimulation procedures, the surgeon's posture can vary, including sitting and/or standing conditions with/without arm rest, and no magnification of the operating theatre is required. In these conditions, 1mm peak-to-peak hand tremor can be considered, thus defining the pointing accuracy (1mm) during free-hand executions.

The need to define a contact safety requirement is due to the fact that large levels of indentation, up to possible penetration, may cause brain tissue's damage. This requirement can be defined in relation to the mechanical properties of the brain soft tissue, which, similarly to other biological tissue, is a viscoelastic, non-linear and anisotropic material (Van Dommelen et al. 2009). Non-penetration indentation experiments reported interaction forces below 0.2N (indentation up to 10mm) (Wittek et al. 2008) and below 0.3N (indentation up to approximately 4mm) (Miller et al. 2000) respectively on in-vitro and in-vivo swine brain. Comparable median contact forces (0.03-0.18N) were reported on human cadaveric brain for retraction tasks (up to 5mm) (Marcus et al. 2014). The puncturing force, i.e. the minimal force required to penetrate the tissue, strictly depends on the dimension of the surgical tool and on the indentation velocity (Abolhassani et al. 2007). Experiments on in-vitro swine brain reported puncture of the pia mater at the needle displacement of 7-10mm (Wittek et al. 2008).

## 1.3 Human robot cooperation in surgery

### 1.3.1 Shared control: impedance/admittance causality[1]

When the manipulator has to interact with the so called environment (i.e. user and/or soft tissues interaction), it is necessary that the robot is controlled to achieve specific desired dynamic behaviors, e.g. providing the force needed to overcome the resistance of the environment or to comply with it, assuring the system stability.

[1] Contribution to Ferrigno G., Pedrocchi A., De Momi E., Ambrosini E., **Beretta** E., chapter E1 "Medical Robotics" in "The Handbook of Electronic Medicine, Electronic Health,Telemedicine, Telehealth and Mobile Health".

Among different control approaches (Villani and Schutter, 2008), “indirect force control” schema achieve force control via motion control, defining the relationship between effort and motion about a nominal end effector trajectory, i.e. virtual impedance of the manipulator. The desired compliant dynamic behavior of the manipulator can be selected to correspond to various manipulation task objectives. We define a robot as "controlled in impedance causality" (torque-based impedance control) if it reacts to motion deviation by generating forces, while we define it as "controlled in admittance causality" (position-based impedance control) if it robot reacts to interaction forces by imposing a deviation from the desired motion (where the robot speed is the controlled variable). The first approach is better suited to keep contact forces small and for application where manipulation gravity loads are small and the motion is slow (Lawrence, 1988). The precise dynamic manipulator model needs to be available and the joint inner loop must be provided at high rate. Conversely, the second approach focuses more on desired force tracking control (Zeng and Hemami, 1997). It suffers from the inability to provide very “soft” impedance, while it is fitting in cases where stiff joint position control is required, e.g. for high accuracy positioning in specific Cartesian direction (Lawrence, 1988).


**Figure 1.4** Hands-on scenario for open-skull neurosurgery. The surgeon manually guides the surgical instruments, fixed to the robotic assistant, and operates next to the patient.

### 1.3.2 Cooperatively controlled robots

Cooperatively controlled robots can supplement, augment, and improve human performance during the execution of surgical tasks (Singer and Akin, 2011). In cooperative/hands-on robotic surgery (Davies et al. 2006), the surgeon manually guides the surgical instruments, fixed to the robotic assistant, and operates next to the patient, sharing the same working space with the manipulator (Figure 1.4).

Hands-on robotic devices were introduced in surgery in the past few years to partially overcome the disadvantages of the autonomous and the tele-manipulation systems already in use (Davies et al. 2004). Differently from the autonomous control mode, in which the manipulator carries out a pre-planned sequence of motions with the surgeon acting as an observer (off-button in case of emergency), hands-on devices do not substitute completely the operator but share the control of the surgical tool, leaving the surgeon in charge of the procedure. Moreover, hands-on robotic systems preserve the familiar interface of the surgeon, who is alongside the manipulator acting on the patient in the operating room, with respect to the tele-manipulation systems, which involve a master console operated by the surgeon. In fact, the latter require considerable concentration from the operator, and even though magnification and scaling of motion is possible, the procedure can be very tiring and time-consuming (Davies et al. 2004). Also, the introduction of haptic feedback, i.e. the sense of touch, in these system is under debate (Okamura, 2009) (Wagner and Howe, 2007).

Cooperative robotic systems are currently used in orthopaedic surgery, in retinal surgery and in neurosurgery. In orthopeaedic surgery, the robotic assistant is used to define virtual geometrical constraints on the hard tissue (Jakopec et al. 2001), that limit the motion of the surgical instrument, allowing for a more precise and reliable placement of the prosthesis with respect to the conventional procedures (Davies et al. 2007). Robotic arms with back-drivable joints are particularly suited, giving the surgeon a direct involvement in the procedure and allowing speeding up the cutting process (Davies et al. 2006). Examples of commercial systems for orthopaedic surgery are the RIO® Robotic Arm Interactive Orthopedic System (Mako Surgical Cop, Ft. Lauderdale, FL) (Pearle et al. 2009) and the ROBODOC ® Surgical Assistant (Curexo, Fremont, CA) (Nakamura et al. 2010). Retinal

surgery is a highly demanding surgical procedure, which requires micro-scale positional accuracy in a limited operating area and reduced contact forces for a safe interaction with the soft tissues. Cooperative manipulation systems based on admittance control, e.g. the Steady-Hand system (Uneri et al. 2010), and hand-held devices, e.g. the Micron system (MacLahlan et al. 2012), were proved to be very effective for precise motion control, providing hand tremor filtering and force feedback enhancement.

The use of the cooperative control mode in neurosurgery is currently limited to keyhole approaches. Cooperatively controlled needle insertion devices (De Lorenzo, Koseki et al. 2013) were developed for keyhole procedure, in order to provide the user with haptic feeling required to detect changing tissue properties of subsurface structures at different depths. During neuroendoscopic procedures, cooperatively controlled robotic assistant can be used as an instruments holder implementing RCM constraints. An example is the Rosa$^{TM}$ (MedTech, Montpellier, France) system, which provides higher mechanical accuracy with respect to standard stereotactic frames (Lefranc et al. 2014).

## 1.4 Our scenario: hands-on robot for brain mapping

It is hypothesized that the introduction of a cooperatively controlled robotic system to assist brain targeting tasks would provide increased positional accuracy and reduce the surgeon's fatigue during the holding phase, when the tool is in contact with the brain tissue. Moreover, the use of a robotic assistant could allow the acquisition of the target positions and guide the surgeon towards the recorded sites, in order to perform repetitive instrument's placements with high accuracy.

Brain cortex stimulation procedures are performed multiple times in different steps of the surgical intervention (generally 3-4 times for 10-15minutes). Thus, assisted surgical targeting tasks would require the repetitive execution of wide maneuvers from/to a home robotic configuration. Moreover, the pointing accuracy requirement in open-skull neurosurgery (1mm) is not as demanding as in microsurgical applications, e.g. micrometer position scale in vitreoretinal eye surgery (Uneri et al. 2010) (MacLahlan et al. 2012). In this context, a highly compliant cooperative manipulator is desirable to promptly react to

the applied forces without resisting to the surgeon's guidance during the target approaching on wide trajectory. Thus, a torque-based impedance controller is suited to provide a "soft" behavior of the manipulator when the tool is far away from the surgical area of interest.

The hands-on robotic assistant should provide:

- high maneuverability and compliance for an intuitive guidance during wide motions, reducing the user's efforts to guide the robot from/to resting configurations;
- high accuracy near the stimulation sites for the stable placement of the surgical instrument, filtering hand tremors;
- safe contact of the surgical tool with the underneath tissue, preventing any damage to the tissue during indentation;
- high consistency and reproducibility across different measurements throughout the same procedure and among patients operated on consecutively.

## 1.5 Aim and structure of the work

The aim of the present work is the development of new methodologies for human-robot and robot-tissue interaction control, specifically designed to augment surgeon's skills during cooperatively assisted targeting tasks on soft tissues (such as during brain mapping procedures). The objectives of this work are therefore to:

(i) investigate the best control strategy for a comfortable and effective cooperation during patient targeting approaching;

(ii) investigate the best control strategy for a safe and stable placement of surgical instruments on soft tissue during the tool placement.

(iii) preliminarily study the feasibility of the proposed impedance control approaches with a pool of expert neurosurgeons for brain cortex stimulation procedures.

In order to address all presented issues, this work is organized in chapters. (**Chapter 1**) The clinical context and the background literature is presented and discussed. The clinical requirements for brain cortex stimulation procedures in open-skull neurosurgery is defined together with the motivations for an hands-on robotic assistive device. (**Chapter 2**) A novel variable damping control is designed to enhance the performance of the surgical hands-on

robotic assistant in terms of ease of use and intuitive guidance during targeting tasks, guaranteeing the respect of the clinical accuracy on the target. The experimental evaluation of this and two well-known impedance controllers with fixed dynamic parameters is carried out with a flexible joint redundant robot during predefined reaching tasks towards registered targets on a calibration board. (**Chapter 3**) A torque controller with non-linear force feedback is proposed, in order to investigate if augmented haptic perception provided to the operator is a relevant factor during the instrument's placement on the soft tissue. This approach is experimentally validated using brain-mimicking gelatin phantoms with a group of non-expert users. (**Chapter 4**) A group of novice and expert neurosurgeons were enrolled to quantitatively and qualitatively evaluate the performances of the proposed cooperative control schema (singularly and in combination) in a realistic scenario for brain cortex stimulation procedures. (**Chapter 5**) The conclusion, scientific and clinical implications, and future sights of this work are finally reported and discussed.

# Chapter 2

# Space Variable damping control for surgical targeting tasks[2]

It is hypothesized that hands-on robotic assistants can be used in surgery for the repetitive execution of targeting/reaching tasks, which require one to smoothly move a tool inside a working area and to keep it in an arbitrary, stable position with high accuracy. Transparency, which quantifies the ability of a robot to follow human movements without any human-perceptible resistive forces, is one of the major issues in the field of human robot interaction for assistance in manipulation tasks (Jarrassé et al. 2008). On the contrary, the ability to approach a target with high accuracy and then keep the tool in a stable position depends on the robot's ability to apply resistance against environmental disturbances.

During brain cortex stimulation in open-skull neurosurgery, varying levels of positional accuracy are required in the operating field, depending on the patient's position and on the surgical area of interest. Also, guidance motions along wide trajectories (from/to resting configuration of the robotic device) are foreseen in a procedure that accomplish different manual and assisted steps in the surgical workflow (Paragraph 1.4). In order to respect the clinical accuracy requirements of the procedure, while increasing the transparency of the system, the surgical robotic assistant should be able to automatically adapt its dynamics during the guidance in the operating theatre.

In this chapter, a novel variable damping controller is designed to enhance the performance of the surgical hands-on robotic assistant in terms of ease of use, intuitive guidance and effectiveness during targeting tasks. The proposed autonomous adaptation

[2] A journal paper on this work has been accepted for publication in the *International Journal of Advanced Robotic System* as **Beretta E**, De Momi E, Rodriguez y Baena F, Ferrigno G. Adaptive Hands-on Control for Reaching and Targeting tasks in Surgery.

criterion is based on *a priori* knowledge of the location of the surgical site. The performance of the proposed controller is comparatively assessed with respect to two well-known impedance controllers with fixed dynamic parameters, identified as the most transparent and the optimal constant damping controllers. The experimental evaluation was carried out with a flexible joint redundant robot during predefined reaching tasks towards registered targets on a calibration board. The applicability of the presented approach in a surgical scenario for brain cortex stimulation procedures, in which the surgical targets are not *a priori* known, would be discussed and evaluated in Chapter 4.

## 2.1 Related work

Selective and adaptive impedance control is the skillful and energy-efficient strategy humans use to learn how to interact with unstable physical environments (Burdet et al. 2001). During the past few years, adaptation criteria that mimic the human arm's behavior were implemented into impedance control strategies for autonomous or tele-operated robotic systems. Human-like learning controllers, derived from the minimization of instability, motion error and effort, were developed for tasks involving interactions with unknown environments (Kadiallah et al. 2012) (Ganesh et al. 2010) (Ganesh et al. 2012) (Yang et al. 2011). The question of how to adjust the compliance of the manipulator during a cooperative task has been addressed in the field of robot learning from demonstration (Kronander and Billard, 2013), where the human operator teaches compliance variation by physically interacting with the robot during the execution of a specific task.

Different variable impedance controllers for human-robot cooperation were presented for surgical (Kazanzides et al. 1992), industrial (Ikeura and Inooka, 1995) (Ikeura et al. 2002) (Erden and Marić, 2011) and assistive robotics (Duchaine and Gosselin, 2007) (Tsetserukou et al. 2007) (Tsumugiwa et al. 2002) (Duchaine et al. 2012) (Nishiwaki and Yano, 2008) applications. The damping factor of the impedance controller was changed with respect to a threshold based on the speed of manipulation by direct switching (Ikeura and Inooka, 1995), by time dependent functions (Ikeura et al. 2002) or by linear variation

(Erden and Marić, 2011). Conversely, the robot impedance was changed in response to the user's force applied at the guidance contact point (Kazanzides et al. 1992) (Duchaine and Gosselin, 2007) (Tsetserukou et al. 2007). More intuitive and stable human-robot cooperation was accomplished when the impedance of the manipulator was modulated with respect to an estimate of the unknown human arm stiffness in (Tsumugiwa et al. 2002) and/or of the human intention of motion (Duchaine et al. 2012). Finally, in (Nishiwaki and Yano, 2008), the impedance of a meal assistance robot is changed with respect to the end-effector position, considering a pre-defined potential field of the obstacles in the workspace, around which the velocity of the robot must be restricted.

It was also shown that the reactive model of a manipulator can be approximated to a second order dynamic system, where the effect of the stiffness parameter is negligible (Ikeura and Mizutani, 1998), thus allowing a robotic arm to be controlled as a (simpler) damping system. A low damping coefficient allows fast system reactions to any applied forces, while a high damping parameter is useful to prevent overshoot, reducing the virtual inertia of the system in situations where the human intention is aimed at decelerating and stopping at a particular point in the robot workspace (Tsumugiwa et al. 2002).

The variable impedance approach based on the end-effector position is appropriate for the brain cortex stimulation scenario, due to the varying accuracy and safety requirements in the operating theatre, which depend on the position of the patient and thus of the surgical area of interest. Also, the impedance would not depend on the characteristics and weight of the surgical tool as would be the case in (Duchaine and Gosselin, 2007) (Tsetserukou et al. 2007) (Tsumugiwa et al. 2002) (Duchaine et al. 2012). Differently from (Nishiwaki and Yano, 2008), where a computational demanding potential field is computed to describe an environment assumed to be static, in this work a space variable (SV) damping criterion is presented to build an intra-operative "accuracy map" based on the knowledge of the surgeon's intention of motion (i.e. the position of the surgical target at the end of the reaching gesture).

# 2.2 Material and Methods

## 2.2.1 Impedance controlled robot model

During hands-on targeting execution, the robotic assistant must responsively react to the forces and torques applied by the operator when the tool is far away from the target, while increasing the resistance to the guidance motion during the final approach, thus improving the accuracy with which a target is intersected. An impedance controller in the task space (Albu-Schäffer et al. 2004) computes the desired Cartesian forces/torques $\mathbf{f}_C = [\mathbf{f}, \boldsymbol{\tau}]$ based on the predefined dynamic behavior of the robot:

$$\mathbf{f} = \mathbf{K}_P(\mathbf{x}_d - \mathbf{x}) + \mathbf{D}_P(\dot{\mathbf{x}}_d - \dot{\mathbf{x}}) \tag{2.1}$$

$$\boldsymbol{\tau} = \mathbf{K}_R(\boldsymbol{\alpha}_d - \boldsymbol{\alpha}) + \mathbf{D}_R(\dot{\boldsymbol{\alpha}}_d - \dot{\boldsymbol{\alpha}}) \tag{2.2}$$

where $\mathbf{K}_C = [\mathbf{K}_P, \mathbf{K}_R]$ and $\mathbf{D}_C = [\mathbf{D}_P, \mathbf{D}_R]$ are the Cartesian stiffness and damping parameters of the arm respectively (prismatic (P) and rotational (R) components), $\mathbf{x}$ and $\mathbf{x}_d$ are the current and desired position of the control point and $\boldsymbol{\alpha}$ and $\boldsymbol{\alpha}_d$ are the current and desired orientation angles of the robot end effector. The dynamic of the robot is compensated with a feed forward model-based torque controller, i.e. gravity and Coriolis-centrifugal terms.

In order to generalize the approach to redundant manipulators (Figure 2.1), the dynamic recursive null-space formulation (Sentis and Khatib, 2005) is used to combine the Cartesian impedance behavior with a damped posture strategy, in which the torque commands are computed as:

$$\boldsymbol{\gamma}_J = -\mathbf{D}_J \dot{\mathbf{q}} \tag{2.3}$$

where $\dot{\mathbf{q}}$ is the actual joint velocity and $\mathbf{D}_J$ is the joint damping parameter. Thus, the combined torque commands are computed with the recursive null-space formulation as follows:

$$\boldsymbol{\gamma} = \mathbf{J}_C{}^T \mathbf{f}_C + \mathbf{N}_C{}^T \boldsymbol{\gamma}_J \tag{2.4}$$

where $\mathbf{J}_C$ is the Jacobian of the linear and angular Cartesian velocities at the control point and $\mathbf{N}_C = \mathbf{I} - \mathbf{A}^{-1}\mathbf{J}_C^T(\mathbf{J}_C\mathbf{A}^{-1}\mathbf{J}_C^T)^{-1}\mathbf{J}_C$ is the dynamically consistent null-space of $\mathbf{J}_C$ computed with the mass matrix $\mathbf{A}$ of the robot.

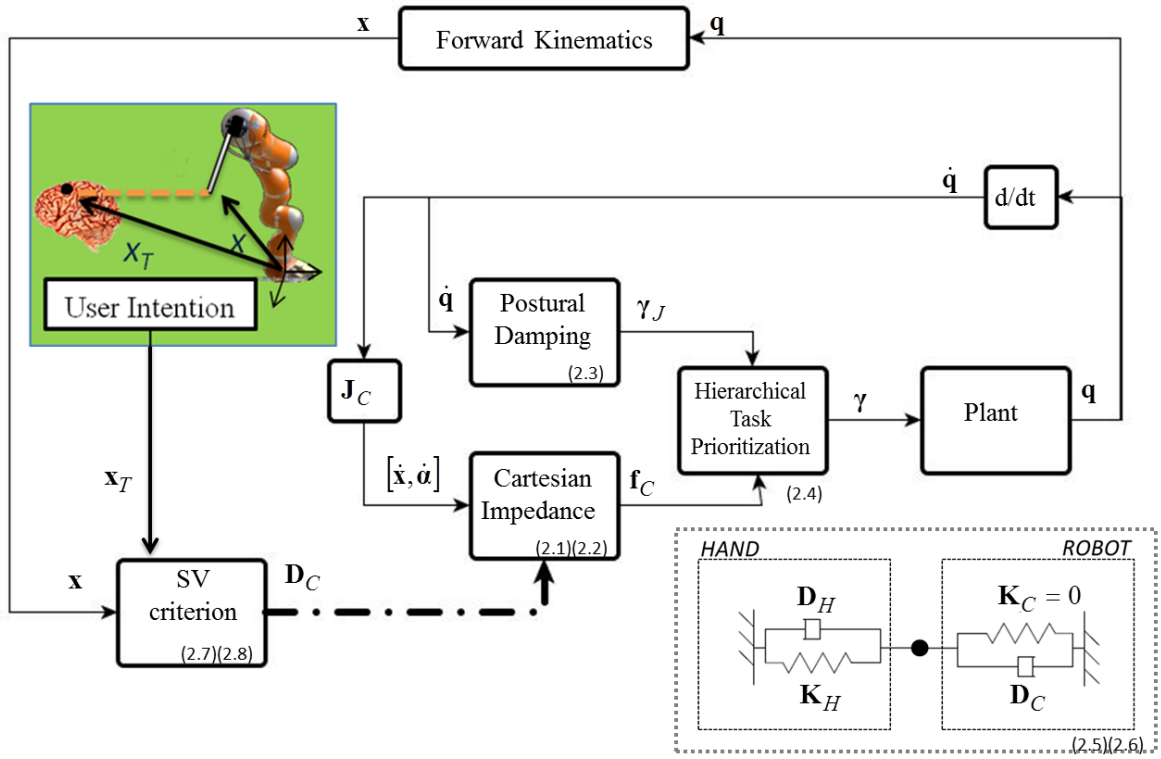


**Figure 2.1** Scheme of the Space Variable damping controller and of the human-robot contact model. The hierarchical task prioritization approach combines the commands computed with the Cartesian impedance controller (null robotic stiffness $\mathbf{K}_C$) with the postural damping commands $\boldsymbol{\gamma}_J$ in the joint space. The Space Variable criterion varies the Cartesian damping parameter $\mathbf{D}_C$ depending on the actual position of the control point $\mathbf{x}$ and on the known position of the target $\mathbf{x}_T$. The actual Cartesian velocities ($\dot{\mathbf{x}}, \dot{\boldsymbol{\alpha}}$) are computed from the actual joint velocities ($\dot{\mathbf{q}}$) with the geometrical Jacobian $\mathbf{J}_C$. The gravitational and Coriolis-centrifugal terms of the feed forward robot's dynamic compensation are not reported.

### 2.2.2 Interaction model

One of the theories on movement control is that the central nervous system guides joint movements through an equilibrium-point control (Bizzi et al. 1992), where the virtual point is determined by the muscle force used to maintain a limb position. Thus, a mass-spring-damper system can be used to model the dynamics of the user's hand on a single-point of contact during the interaction (Marayong et al. 2006). Supposing that the hand maintains contact with the manipulator at all times, the robot and the hand are at the same position (**x**) and orientation (**α**) and the coupled interaction model between the manipulator and the human hand, the dynamics of which are represented by the stiffness ($\mathbf{K}_H = [\mathbf{K}_{P,H}, \mathbf{K}_{R,H}]$) and damping ($\mathbf{D}_H = [\mathbf{D}_{P,H}, \mathbf{D}_{R,H}]$) matrices, is shown in Figure 2.1. The mass terms can be neglected as in (Roveda et al. 2013), when a reasonable task bandwidth of 5Hz is considered in the damped case, and the actual stiffness of the coupled system is given by the parallel equivalent of the two individually (Duchaine and Gosselin, 2008). If the virtual stiffness of the manipulator is set to zero ($\mathbf{K}_C = 0$, not to become an additional load sensed during the cooperation (Ikeura and Inooka, 1995)), the coupled interaction model can be approximated to:

$$\mathbf{f}_{ext} = \mathbf{K}_{P,H}(t)(\mathbf{x}_d - \mathbf{x}) - (\mathbf{D}_{P,H}(t) + \mathbf{D}_P)\dot{\mathbf{x}} \tag{2.5}$$

$$\boldsymbol{\tau}_{ext} = \mathbf{K}_{R,H}(t)(\boldsymbol{\alpha}_d - \boldsymbol{\alpha}) - (\mathbf{D}_{R,H}(t) + \mathbf{D}_R)\dot{\boldsymbol{\alpha}} \tag{2.6}$$

where the stiffness $\mathbf{K}_H$ and damping $\mathbf{D}_H$ parameters of the hand are unknown and time-varying. The damping characteristics of the hand is assumed to be implicitly adapted by the user to ensure passivity of the coupled system in relation to the applied human stiffness during the assisted guidance (Duchaine and Gosselin, 2008).

### 2.2.3 Space Variable Damping Controller

In order to enhance the human-robot interaction during hands-on robotic surgery, a variable damping controller varies the viscosity characteristics of the manipulator with the isotropic SV criterion, which is based on *a priori* knowledge of the surgical targeting

gesture. Assuming that the target position is known in the robot base reference frame, both the translational $\mathbf{D}_P$ and the rotational $\mathbf{D}_R$ damping matrixes vary according to the distance ($d$) between the actual position $_{\mathbf{x}}$ of the control point and the known position of the target, so that higher damping is achieved only in areas of the robot workspace where high positional accuracy is required. A sigmoid spatial modulation (Figure 2.2) is considered and applied independently in each direction of motion:

$$\mathbf{D}_P(d) = \underline{\mathbf{D}}_P + (\overline{\mathbf{D}}_P - \underline{\mathbf{D}}_P)\frac{1}{1+e^{\beta(d-m)}} \tag{2.7}$$

$$\mathbf{D}_R(d) = \underline{\mathbf{D}}_R + (\overline{\mathbf{D}}_R - \underline{\mathbf{D}}_R)\frac{1}{1+e^{\beta(d-m)}} \tag{2.8}$$

where $\underline{\mathbf{D}}_{P,R}$ and $\overline{\mathbf{D}}_{P,R}$ are the lower and upper boundaries of the prismatic and rotational damping parameters respectively, $m$ is a spatial threshold that defines the isotropic area around the target in which the damping is increased and $\beta$ is a scalar parameter that defines the damping rate of change of the sigmoid function.

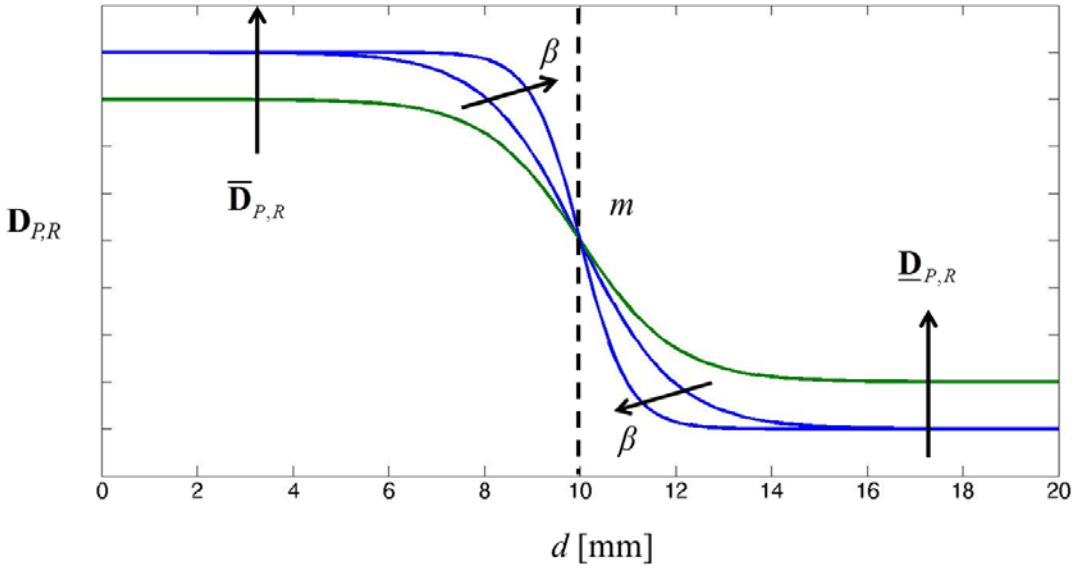


**Figure 2.2** Sigmoidal modulation applied to the prismatic ($\mathbf{D}_P$) and rotational ($\mathbf{D}_R$) damping parameters of the manipulator according to the actual distance ($d$) from the target.

### 2.2.4 Experimental Protocol

The SV damping modulation criterion of the proposed controller was experimentally evaluated using the LWR4+ (Kuka, Augsburg, Germany), a 7 Degrees-of-Freedom (DoFs) flexible joint manipulator with joint torque sensors (±1.5Nm static friction), which features 0.05mm repeatability (as per datasheet) and ≈1mm accuracy (Stein et al. 2009). The effectiveness of the proposed SV damping controller was evaluated with respect to two constant isotropic damping controllers:

- Gravity Compensation (GC): $\mathbf{D}_P = \underline{\mathbf{D}}_P$ =0Ns/m and $\mathbf{D}_R = \underline{\mathbf{D}}_R$ =0Nms/rad, i.e. a constant under-damped interaction; if the robot's dynamic were ideally compensated, the GC controller would allow the most transparent interaction with the user;
- Constant Optimal damping (CO): $\mathbf{D}_P = \overline{\mathbf{D}}_P$ =30Ns/m and $\mathbf{D}_R = \overline{\mathbf{D}}_R$ =30Nms/rad, i.e. a constant over-damped interaction; the robotic damping coefficient were computed to mimic the human arm damping effect ($\mathbf{D}_H = \sqrt{\mathbf{K}_H}$)(Duchaine and Gosselin, 2008), considering a mean human hand stiffness equal to 900N/m according to the stiffness range defined in (Marayong et al. 2006) during soft-normal-hard gripping.

The isotropic sigmoid spatial modulation (2.7)(2.8) of the SV controller was applied, varying the damping between the boundaries ($\underline{\mathbf{D}}_{P,R}$ and $\overline{\mathbf{D}}_{P,R}$) defined for the fixed parameter controllers. The spatial parameters of the SV criterion were heuristically determined ($m$ equal to 50mm and β equal to 50m$^{-1}$) based on the qualitative considerations of an expert user during the repetitive execution of targeting gestures. The above-mentioned control schemes were implemented as modules of the Whole Body Control library (Stanford) (Philippsen et al. 2011), i.e. a torque control framework with hierarchical task prioritization (Sentis and Khatib, 2005). The robotic control system was implemented in a custom define Open RObot COntrol System (OROCOS) and Robot Operating System (ROS) architecture and controlled in a real-time environment guaranteed by a Xenomai patched Linux kernel. Torque commands depending on the variable damping parameter were computed at 200Hz, while internally updated at 1KHz from the LWR controller (Albu-Schäffer et al. 2004).

A bespoke linear tool was mounted on the robot flange, as shown in Figure 2.3. A reference frame (RF) with the origin coincident with the tip of the linear tool (tool center point - TCP) and the z-axis coaxial with the tool's principal axis ($\mathbf{RF}_{TCP}$) was defined with respect to the flange reference frame ($\mathbf{RF}_F$) using a pivoting procedure. Tests were performed on a calibration board, mimicking the target approaching gestures of an open-skull neurosurgical procedure. The board is realized with a rapid prototyping machine (accuracy 0.5mm) and a 4x4 grid of 2cm equally spaced points is realized on the surface, together with five 3mm diameter calibration divots. The user's motion intentions were constrained to provide a ground truth for the evaluation of the controllers' performance: one of the grid points was chosen as the intended target of the assisted gesture and its position in the robot base reference frame $\mathbf{x}_T$ was computed through a rigid registration procedure (Horn, 1987) on the board divots (fiducial registration error (Fitzpatrick and

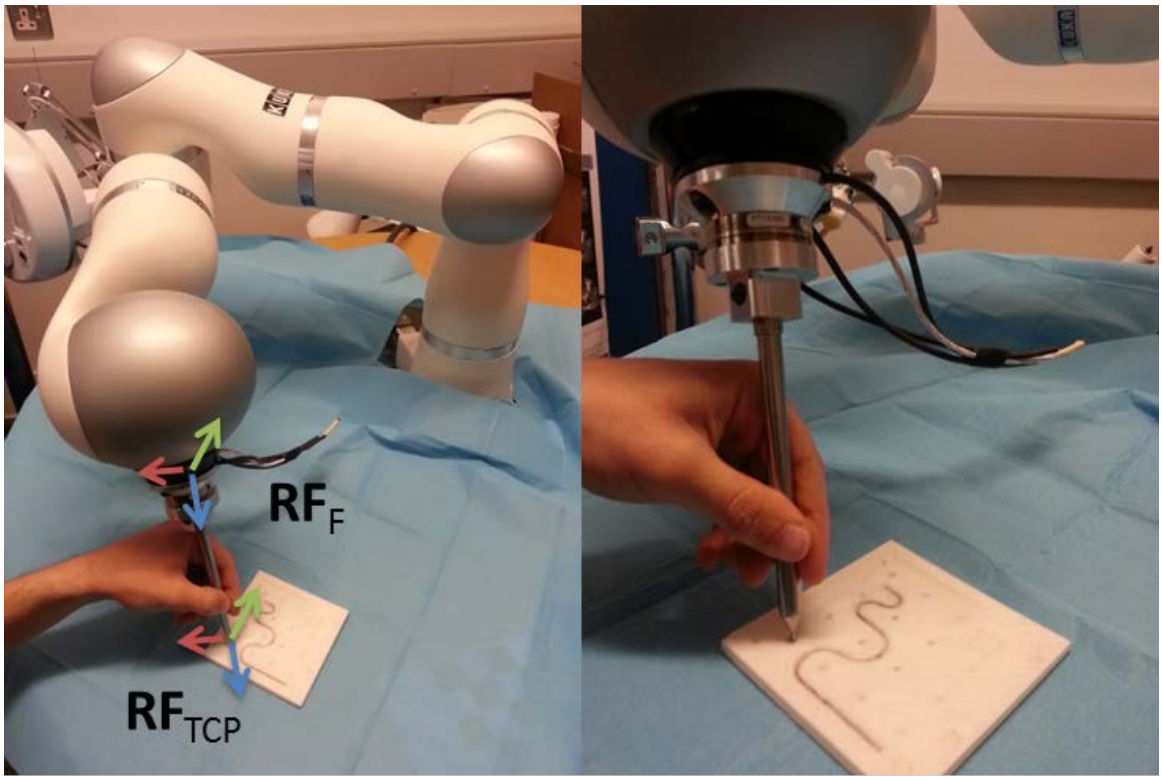


**Figure 2.3** Experimental setup with the LWR4+ robot and the target calibration board. The reference frames of the robot flange ($\mathbf{RT}_F$) and of the tool central point ($\mathbf{RF}_{TCP}$) are also reported in RGB convention (red is *x*-axis, green is *y*-axis and blue is *z*-axis).

West, 2001) equal to 1.1mm). Fifteen non expert users were asked to perform 12 robotic assisted targeting gestures towards the predefined target on the calibration board, with each of the three GC, CO and SV controllers in a randomized order. During each trial, the initial joint positions of the manipulator are varied randomly both in terms of the Cartesian pose $\mathbf{RF}_{TCP}$ (distance from target greater than 300mm) and the position of the elbow, in order to evaluate the controllers in arbitrary dynamic configurations.

### 2.2.5 Performance Indexes

During the randomized trials, the joint configurations, the Cartesian pose of the TCP and the exerted Cartesian forces estimated from the external joint torques (low pass filter with cut-off frequency between 100-300Hz) were provided by the internal KUKA controller (at 200Hz). The time derivatives of the Cartesian TCP position, e.g. Cartesian velocities, were computed with a best-fit First Order Adaptive Window Recursive filter (Janabi-Sharifi et al. 2000). Based on these information, the performances of the constant and variable damping controllers were evaluated in terms of:

- target pointing error ($E_T$), computed as the root mean square distance between the known calibrated target position and the actual TCP position evaluated at the end of the motion (window equal to 0.5s);
- target approaching execution time ($T$), evaluated starting from a 100mm distance from target, in order to compensate for different initial path length;
- mean norm of the exerted Cartesian forces ($F_{mean}$) during the cooperation, in order to quantify the transparency of the system and thus the user's efforts;
- maximum norm of the acceleration ($Acc$) computed at the contact point during the cooperation, in order to quantify the reaction capabilities of the system;
- zero crossing index ($ZC$), evaluated on the velocity measured at the TCP when the distance from the target is less than 10mm, in order to quantify the number of speed direction changes experienced while approaching the target;
- motion smoothness ($S$), evaluated as the inverse of the root mean square jerk, i.e. third derivative of the TCP positions, during the target approaching (distance from the

target less than 100mm).

The mean behavior of each user was evaluated during the gesture execution with the GC, CO and SV controllers over 10 trials (the first and second trials were excluded in order to account for user's accommodation). For each user, the median value and the first and third Inter Quartile Ranges (IQR 50%-25%; IQR 75%-50%) and the mean and the standard deviation were computed over different trials respectively for the discrete *ZC* index and all the others performance indexes. A comparative analysis of the performance of the GC, CO and SV controllers among different users was carried out using the Friedman paired test with Bonferroni-Holm correction ($p<0.05$) (Holm, 1979).

## 2.3 Results

Evaluation of the performance indexes for the assisted targeting gestures is reported in Figure 2.4. The target pointing error ($E_T$, Figure 2.4a) of CO and SV controllers (mean value below 1.3 mm) is comparable to the experimental accuracy of the LWR4+ manipulator reported for repetitive motions (Stein et al. 2009), while the accuracy of the GC controller is significantly reduced (by almost 50%) resulting in a mean target pointing error equal to 2.2mm. The approaching execution time (*T*, Figure 2.4b), computed on the last 100mm trajectory towards the target, is comparable among all the three controllers (mean value around 6s). Figure 2.4c shows that the mean norm of the exerted forces ($F_{mean}$) applied during the cooperative interaction with the SV controller (mean value equal to 2.6N) are greater than with the GC controller (mean value equal to 1.2N) and reduced with respect to the CO controller (mean value equal to 4.1N). As shown in Figure 2.4d, the accelerations (*Acc*) allowed while cooperating with the SV controller are comparable to those for the GC controller (mean value greater than $1 m/s^2$) and significantly higher (around 50%) with respect to the CO controller (mean value below $0.5 m/s^2$). At the same time, the trajectory smoothness (*S*, Figure 2.4e) and the zero crossing index (*ZC*, Figure 2.4f) of the SV controller are comparable to those of the CO controller (respective mean smoothness greater than $0.8 s^3/m$ and median direction changes equal to 4) and reduced by

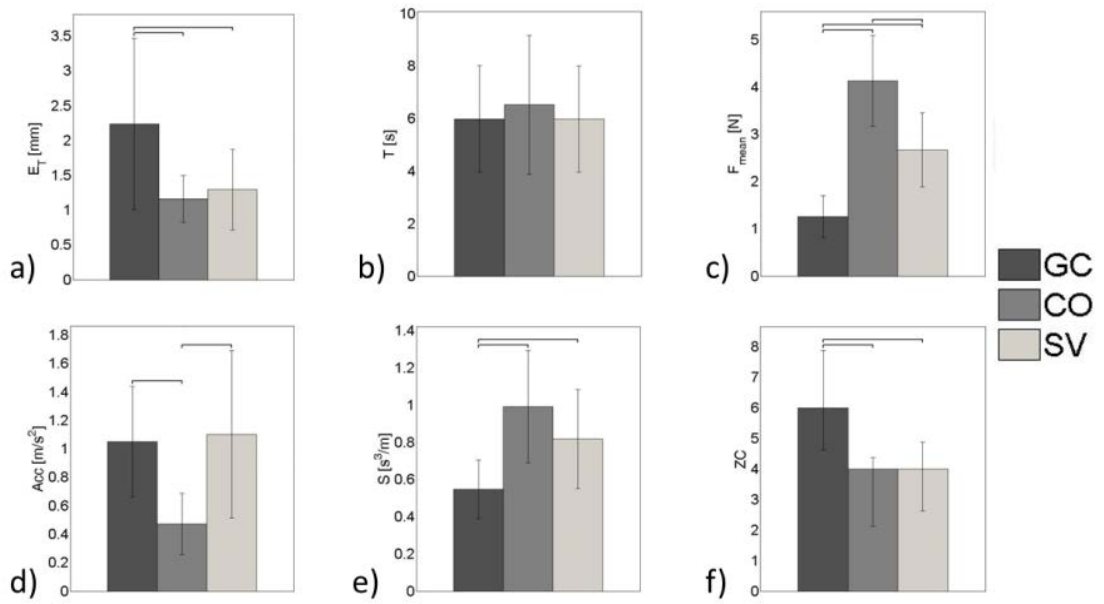


**Figure 2.4** Evaluation of a) pointing accuracy ($E_T$); b) target approaching execution time ($T$); c) mean norm of the exerted Cartesian force at the contact point ($F_{mean}$); d) maximum norm of the acceleration at the contact point ($Acc$); e) motion smoothness ($S$); f) zero crossing ($ZC$) of the three controllers (GC,CO, SV) among the randomized users' group. Vertical bars represent means and standard deviations for each population of the indexes (a)-(e) and median values and quartiles (25% and 75%) for the population of index (f) . Horizontal lines represent statistically significant differences, as determined in Friedman paired test ($p<0.05$) with Bonferroni-Holm correction.

more than 30% with respect to the GC controller (respective mean smoothness below $0.6 s^3/m$ and median direction changes equal to 6).

## 2.4 Discussion

An hands-on variable damping controller is presented to enhance human-robot interaction during targeting gestures, particularly suited for surgical applications. Based on the assumption that the desired position at the end of the assisted motion is known *a priori*, the space variable criterion allows one to modulate the viscosity parameter of the manipulator along the trajectory, and thus to smoothly vary the level of transparency and pointing accuracy of the robotic system according to the target position. During robotic

surgical interventions, this assumption is usually verified thanks to the registration procedures that are performed between the intra-operative space, the robot space and the patient-specific image space (Ferrand-Sorbets et al. 2010) (Hughes et al. 2013), that localize the area of intervention of the patient in the robot base reference frame. Nevertheless, during brain cortex stimulation in neurosurgery (Szelènyi et al. 2010), the stimulation site on the exposed brain cortex is not known *a priori* in the pre-operative phase and changes during the procedure, depending on the surgeon's stimulation intentions. The possible application scenario of the SV controller for brain cortex stimulation procedures, where the surgeon/user is able to configure the damping field of the SV criterion online, based on his/her actual intention of motion through an image-guided navigation system, is presented, evaluated and discussed in Chapter 4.

The SV controller isotropically varies both the translational and rotational damping parameters of the manipulator in a predefined range of values. The user's hand is hypothesized to behave as a spring-damper system with time-variable dynamic parameters (Marayong et al. 2006). Thus, it is realistic to assume that the damping characteristics of the hand are adapted by the user to ensure passivity of the coupled system in relation to the applied human stiffness.

The effectiveness of the proposed SV controller was experimentally evaluated on a pool of 15 non-expert users with respect to both a gravity compensation (0Ns/m, 0Nms/rad) and constant optimal (30Ns/m, 30Nms/rad) damping controllers, the transparency and pointing accuracy of which are maximum respectively. Although far from the real clinical scenario, the experimental tests were performed using a registered calibration board, on which the surgical target was defined and visible to the users, thus constraining the user's pointing intention to be considered as the motion ground truth.

Experimental results showed that the performance of the proposed controller combines the positive features of the gravity compensation controller, i.e. high acceleration capabilities (increased by more than 30% with respect to the constant over-damped scenario), and of an optimal damping controller, i.e. acceptable pointing accuracy (mean target localization error below 1.3mm) and intuitive convergence to the target (the direction changes are reduced by a factor of 30% with respect to the constant under-damped

scenario). Although reduced with respect to the GC controller, the transparency of the system with the SV controller (mean exerted force below 3N) is increased by 40% with respect to the CO controller. Thus, the user's effort during the cooperative task is reduced, though providing comparable pointing accuracy. The smoothness of the assisted trajectory (mean jerk below $1m/s^3$) is guaranteed for all three controllers.

As expected, when the robotic device is controlled to provide the maximum transparency (GC mode), the operator is not able to perform precise motions because of the residual friction of the system (±1.5Nm on joint torques sensors). Conversely, the SV controller was proved more reliable with respect to both the non-ideality of the dynamic robotic model and the time-varying human interaction during the cooperation, guaranteeing the respect of the clinical accuracy requirement (Paragraph 1.2.1).

To be applied to a redundant manipulator, the SV control approach was defined in the framework of the hierarchical task prioritization (Sentis and Khatib, 2005) and combined with a posture damping strategy to control the position of the robotic elbow during the assisted cooperation. The investigation of the potential benefits derived from different null-space control strategies, e.g. the minimization of the residual robot inertia, is not the focus of this work and would be addressed in the future (as discussed in Chapter 5).

In conclusion, the proposed space variable damping controller was shown to be suitable for cooperative targeting tasks that require different levels of position accuracy in the operating field, such as targeting gestures during brain cortex stimulation in open-skull neurosurgery. Enhanced performance is demonstrated by comparison to two fixed parameter controllers, where reaching tasks under laboratory conditions result in reduced targeting error and user effort.

# Chapter 3

# Force Feedback Enhancement for Soft Tissue Interaction Tasks[3]

In open-skull neurosurgery procedures, the contact between the surgical instrument and the underneath tissue must be guaranteed stable, filtering hand tremors, and safe, preventing any damage to the tissue due to indentation (Paragraph 1.4). Additionally, if predictable and/or unpredictable brain motions occur, e.g. respectively due to breathing and pulsatility (Faria et al. 2014) and/or to induced epileptic seizures (De Lorenzo, De Momi et al. 2013), the robotic assistant should be able to compensate them and react safely.

Touch interactions and physical contacts are critical factors during the manipulation of tissue/objects. Haptic feedback in tele-operation and cooperative manipulation systems has been an active area of research for several decades, although its benefits in robotic surgery have not yet been assessed in terms of clinical outcome (Okamura, 2009) and major issues have prevented its use in a commercially available system (Yamamoto et al. 2012) (De Lorenzo, Koseki et al. 2013), e.g. the intrinsic trade-off between stability and transparency and the challenge of sensing forces under cost, biocompatibility and sterilizability constraints. However, force feedback was proved to allow for tissue characterization (Yamamoto et al. 2012) (Dalvand et al. 2014), lower applied forces on tissues (Wagner and Howe, 2007) and reduced unintentional injuries (Demi et al. 2005). In particular, admittance-controlled (position-based impedance control) robotic assistant, guided by the instant feedback of forces measured at the surgical instrument, prevent force-induced damage to soft tissues and reduce the surgeon fatigue both for tele-operated devices, e.g. in heart surgery (Mayer et al. 2007), and for cooperative manipulation systems, e.g. in vitro-

[3] A conference paper on this work has been submitted as **Beretta E**, Nessi F, Ferrigno G, De Momi E. Force Feedback Enhancement for Soft Tissue Interaction Tasks in Cooperative Robotic Surgery

retinal surgery (Uneri et al. 2010) and in assisted needle insertion in keyhole neurosurgery (De Lorenzo, Koseki et al. 2013).

However, standard force-to-motion control schema are not advisable for surgical targeting tasks requiring the repetitive execution of wide maneuvers from/to a home robotic configuration, e.g. during brain mapping procedures (Paragraph 1.4). Robots controlled with low impedance, e.g. the Acrobot system with back-drivable joints for robotic assisted orthopaedic surgery (Davies et al. 2006), allow the natural transmission to the user of the interaction forces with the environment, both for human guidance and/or for tissue contact, without requiring direct force sensing (Albu-Schäffer et al. 2004). Nevertheless, an enhancement of the tool-tissue kinaesthetic information is needed to provide haptic sensation to the user during the manipulation of the brain soft tissue, due to the small ranges of forces involved (Paragraph 1.2.1).

This chapter deals with the design of a non-linear force feedback torque control in order to augment the surgeon's skills during the placement of the surgical instrument with respect to pure visual feedback. The controller parameters were optimized on brain-mimicking gelatin phantoms, which were mechanically characterized to quantitatively evaluate the tissue's damage due to the contact with the tool, thus allowing the definition a safety criterion based on the maximum force and penetration allowed during the indentation. The performances of the robotic assistance with and without force feedback augmentation were comparatively evaluated with respect to freehand task executions, both in terms of effectiveness in reduction of the tissue's indentation force during the target approaching and hand tremor rejection during the holding phase.

# 3.1 Related work

Cooperative manipulation systems based on admittance control proved to be very effective in highly demanding surgical procedures requiring high tool positional accuracy, e.g. vitro-retinal surgery (Uneri et al. 2010) (He et al. 2014) and keyhole neurosurgery (De Lorenzo, Koseki et al. 2013), thus where a "very stiff" dynamic behavior of the robotic device is desirable. Scaled force reflection strategies (Uneri et al. 2010) (Berkelman et al.

2000) were developed for the John Hopkins "Steady-Hand Eye" robot in vitreoretinal surgery, where surgeons are required to perform micro scale maneuvers while safely applying forces that are below sensory perception. In particular, a micro-force guided cooperative control, enforcing a global limit on the forces applied at the robot tool tip and actively guiding the operator towards the direction of lower resistance, proved to be effective in enforcing force limits during membrane peeling tasks (Uneri et al. 2010). Also, sclera contact location and force measurements were recently used to adapt the RCM constrain in a variable admittance controller in order to minimize the eye motion while enabling tool manipulation inside the eye, as well as provide useful sclera force feedback to assist to reposition the eye (He et al. 2014). Force-to-motion control schema with linear force feedback enhancement were implemented also for cooperative assisted needle insertion devices (De Lorenzo, Koseki et al. 2013), thus providing the user with the haptic feeling required to detect changing tissue properties of subsurface structures at different depths.

All the above-mentioned force tracking control approaches exploit the manipulator with high stiffness dynamics and suffer from the inability to provide a "soft" compliant behavior (Paragraph 1.3.1). Torque-based impedance control is better suited to provide the small stiffness and damping desirable in reducing contact forces (Lawrence, 1988). However, robotic mechanical impedance may mask any delicate force arising from the interaction with soft tissues (Okamura, 2004), reducing the user perceivable level (He et al. 2013). In particular, brain interaction forces were reported in the range 0.03-0.3N during indentation up to 5mm (Paragraph 1.2.1). The maximum peak forces during manual and robotic direct assess needle insertion respectively into in-vivo bovine liver and kidney were reported in the range 0.7-0.8N (Maurin et al. 2004).

# 3.2 Materials and Methods

## 3.2.1 Torque control with force feedback enhancement

In order to provide a "soft" dynamic behavior during the cooperative guidance (Lawrence, 1988), a torque control for flexible joint manipulators is used (Albu-Schäffer et

al. 2004). As shown in Figure 3.1, the torque input of the joint state feedback controller ($\boldsymbol{\tau}$) is computed as:

$$\boldsymbol{\tau} = \boldsymbol{\tau}_d + \boldsymbol{\tau}_n + \boldsymbol{\tau}_e \tag{3.1}$$

where $\boldsymbol{\tau}_d$ is the desired torque vector, $\boldsymbol{\tau}_n$ is the feed forward model-based torque vector for the compensation of the robot's dynamic, i.e. gravity and Coriolis-centrifugal terms, and $\boldsymbol{\tau}_e$ is the vector of the external torques applied to the manipulator by the environment. For our study, we assume two different types of environmental interaction ($\mathbf{f}_e$):

- Human interaction forces ($\mathbf{f}_h$): the operator guides the manipulator applying external forces with a single-point contact during the free-motion guidance phase and the instrument's placement phase, depending on his/her unknown intention of motion (Marayong et al. 2006);

- Soft tissue interaction forces ($\mathbf{f}_t$): the compression /indentation reaction of the soft tissue during the instrument's placement phase depends on its viscoelastic mechanical properties (Abolhassani et al. 2007).

Thus, the external torque vector can be written as:

$$\boldsymbol{\tau}_e = \mathbf{J}^T(\mathbf{f}_h + \mathbf{f}_t) \tag{3.2}$$

where **J** is the Jacobian matrix of the manipulator. Non-idealities of the robot dynamic models limit the maximum transparency of the system (Marayong et al. 2006). In fact, residual inertia and friction of the manipulator may mask the delicate interaction forces generated by the contact with the soft tissue during the target placement phase. Thus, a force feedback enhancement loop is required to provide haptic perception during tissue's indentation.

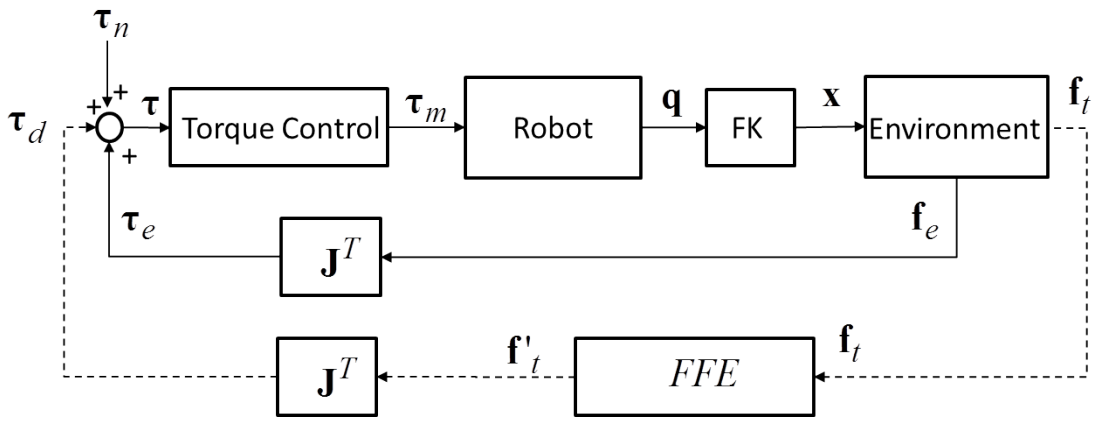


**Figure 3.1** Torque control with force feedback enhancement (FFE). $\boldsymbol{\tau}_m$ is the motor torque vector, $\tau$ is the joint torque vector, **q** is the joint configuration vector and **x** is the Cartesian end-effector position computed with the Forward Kinematic (FK) block. The environment forces ($\mathbf{f}_e$) represents both the operator's hand and the tissue during the cooperative guidance. If the tissue's contact forces ($\mathbf{f}_t$) are directly measured with a force sensor on the instrument, the desired torque vector ($\boldsymbol{\tau}_d$) is computed according to the enhancement strategy (dot line).

When direct measurements of the soft tissue interaction forces $\mathbf{f}_t$ are available, e.g. with a force sensor on the instrument, the non-linear force feedback enhancement (FFE) is computed as:

$$\begin{cases} \mathbf{f}'_t = \rho(\mathbf{f}_t)^n & \left\|\mathbf{f}'_t\right\| < \mathbf{f}_s \\ \mathbf{f}'_t = \mathbf{f}_s & \left\|\mathbf{f}'_t\right\| \geq \mathbf{f}_s \end{cases} \tag{3.3}$$

where $\rho$ is a positive scalar ($\rho$ >0), $n$ is the positive exponent of the polynomial function in the range (0-1], thus enhancing the contrast for small forces (Figure 3.2), and $\mathbf{f}_s$ is a saturation level, which defines the maximum force feedback perceivable from the tissue, thus representing the maximum force the user has to overcome to intentionally penetrate the tissue. The commanded torque vector is then computed as:

$$\boldsymbol{\tau}_d = \mathbf{J}^T(\mathbf{f}'_t) \tag{3.4}$$

Thus, the balance of forces at the contact point results when:

$$\mathbf{J}^T(\mathbf{f}'_t + \mathbf{f}_t + \mathbf{f}_h) = 0 \tag{3.5}$$

$$\mathbf{f}_h = -(\mathbf{f}'_t + \mathbf{f}_t) \approx -\rho(\mathbf{f}_t)^n \tag{3.6}$$

considering the tissue's interaction forces negligible with respect to the augmented forces.

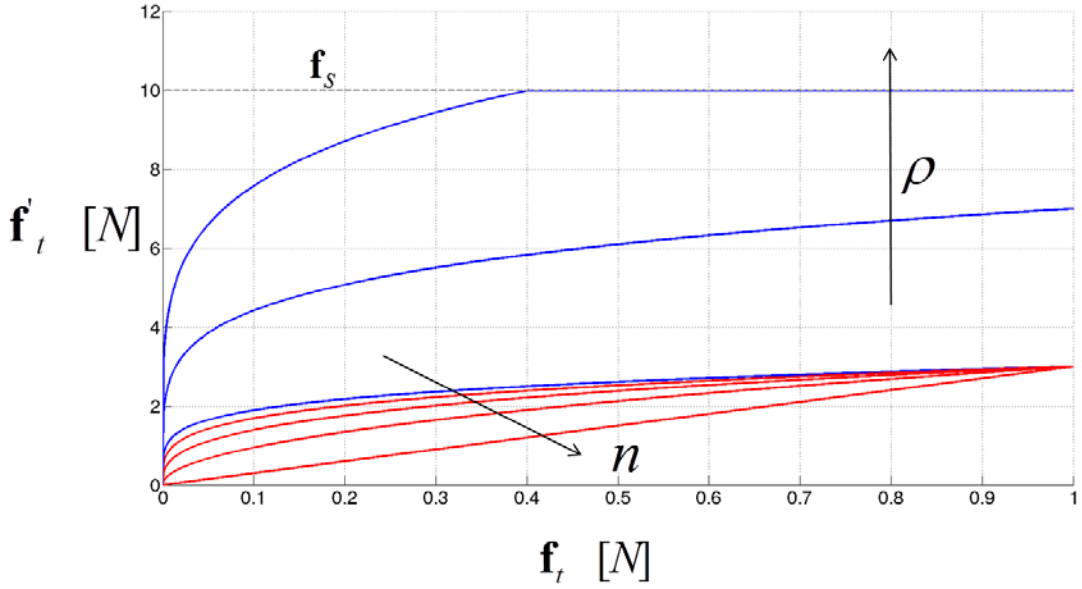


**Figure 3.2** Non-linear force feedback enhancement parameters.

### 3.2.2 Experimental Protocol

The proposed control approach was experimentally evaluated using the LWR4+ robot (features reported in Chapter 2). A 3D printed spherical handle was placed at the end-effector of the LWR4+ manipulator to be grasped by the user during the guidance (Figure 3.3). The forces applied at the end-effector ($\mathbf{f}_e$) were estimated from the external torques measured by the joint torque sensors of the manipulator ($\boldsymbol{\tau}_e$). In order to distinguish between the interaction forces of the human guidance and the soft tissue's indentation, a 6 DoFs Nano43 F/T sensor (ATI Industrial Automation, Apex, NC), which features 1/512N-1/40Nmm resolution in a 9N-125Nmm range, was mounted between the handle and a linear

tool (3mm diameter tip), mimicking the surgical tool used during brain stimulation. The Gamma F/T sensor (ATI Industrial Automation, Apex, NC), which features 1/80N-1/2Nmm resolution in a 32N-2.5Nm range, measured the interaction forces on the soft material's phantoms during free-hand task executions. The Optotrack Certus localization system (Northern Digital Instruments, Ontario, Canada) with active markers (0.1mm accuracy) was used to track the instrument pose ($\mathbf{RF}_{EE}$) and the calibration plate ($\mathbf{RF}_{CP}$) in the camera frame ($\mathbf{RF}_{C}$). The position of the tip of the linear tool ($\mathbf{t}^{EE}$) was computed in $\mathbf{RF}_{EE}$ using a pivoting procedure and a reference frame with the origin coincident with it and the z-axes coaxial with the tool's principal axes ($\mathbf{RF}_{TCP}$) was defined. A 3D-printed calibration plate was rigidly fixed to the load cell and used to define a reference frame with the z-axis coincident with the normal of the plane ($\mathbf{RF}_{P}$) computed in the $\mathbf{RF}_{CP.}$ Closing the kinematic chain on the optical transformations (Comparetti et al. 2014), the tool tip position was obtained in $\mathbf{RF}_{P}$ ($\mathbf{t}_{tcp}$):

$$\mathbf{t}_{tcp} = (T^{CP}{}_{P})^{-1} (T^{C}{}_{CP})^{-1} T^{C}{}_{EE}\, \mathbf{t}^{EE} \tag{3.7}$$

where $T^{A}{}_{B}$ indicates the transformation from $RF_A$ to $RF_B$. Also, the force measurements of the load cell ($\mathbf{f}_{lc}$) were computed in $\mathbf{RF_P}$, using the CAD models of the printed plate.

The robotic control system was implemented in a custom define OROCOS and ROS architecture and controlled in a real-time environment guaranteed by a Xenomai patched Linux kernel. Torque commands were computed at 1 kHz, while the F/T signals were acquired at 2 kHz. The end-effector F/T measurements ($\mathbf{f}_{fs}$) were processed with a notch filter (cut frequency 186.5 Hz, minimum order) to cancel the noise from the robot's fan vibrations. Also, the dynamic of the linear tool was online compensated (Kubus et al. 2007), resulting in a 0.02N accuracy of the force measurements at the end-effector.

Tests were performed mimicking the target approaching gestures of an open-skull neurosurgical procedure using gelatin phantoms with three different concentrations (8, 12, 16 %), that mimic the viscoelastic characteristics of the brain tissues (De Lorenzo et al. 2011). The flat surface of each phantom was calibrated in the robot base reference frame with a least square regression process on 12 points acquired with an optical pointer (root mean square error < 0.5 mm).

The experimental protocol included three phases:

- tissue characterization for contact damage quantification;
- optimization of the FFE controller;
- evaluation of the FFE controller performance.

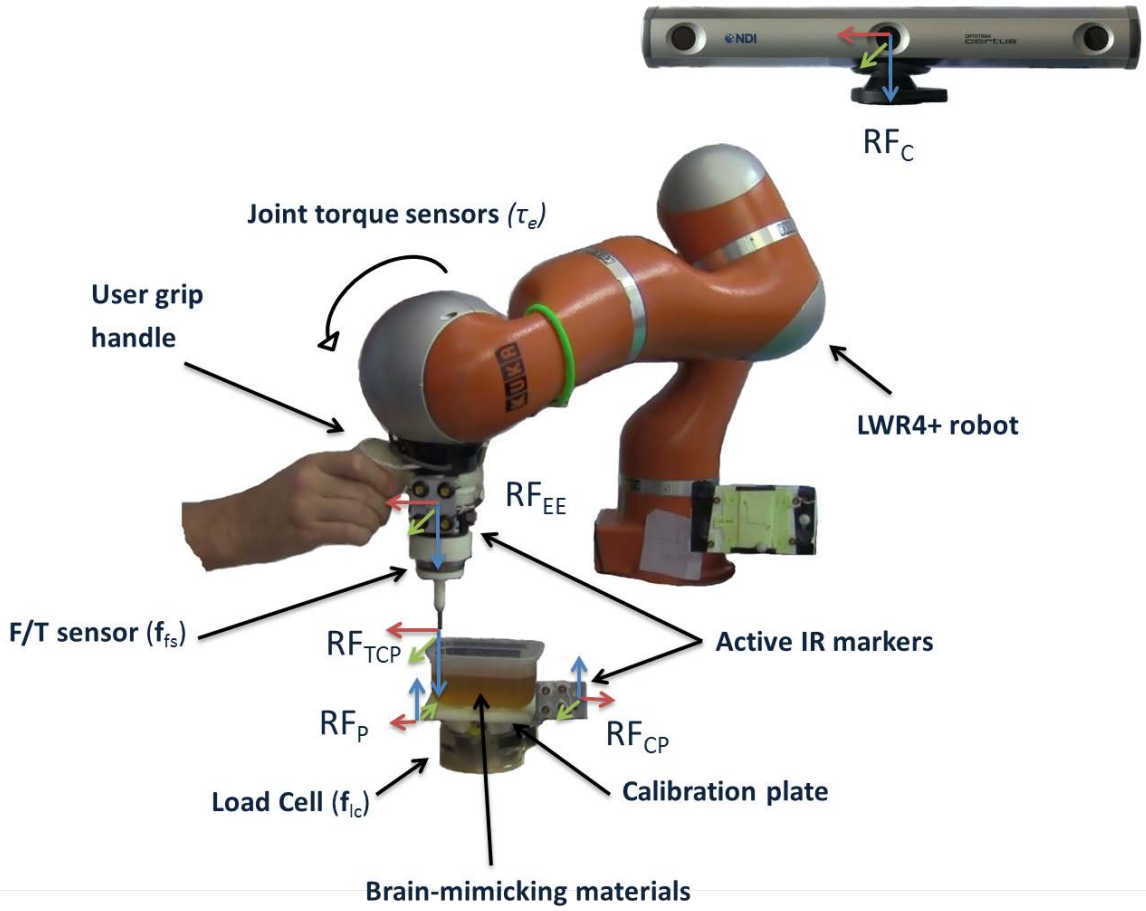


**Figure 3.3** The experimental setup. The reference frames (RFs) of interest are also reported

### 3.2.2.1 Tissue characterization for contact damage quantification

During brain stimulation the surgeon places the stimulators in contact with the brain cortex. Large levels of indentation, up to possible penetration, may cause tissue's damage. In order to quantitatively define in which range of forces penetration occurs, thus

identifying a safety criterion for the gelatin indentation, the gelatin phantoms were characterized in terms of puncturing force ($\bar{\mathbf{f}}_t$) and penetration level ($\overline{p}_t$). The protocol included 8 trials of autonomous robotic tool insertions at different velocities (4-16mm/s) performed for each gelatin at different concentrations (8-16%). Each gelatin phantom was kept for at least 8 hours at a temperature of 5°C before use and changed at every experiment to avoid degradation of the material due to the environmental temperature (25°C). The F/T signals from the end-effector sensor ($\mathbf{f}_{fs}$) were processed with a first order adaptive derivative filter (Janabi-Sharifi et al. 2000) to identify the peak related to the puncturing event.

**Table 3.1** Results for the autonomous tool insertion protocol

| $\bar{\mathbf{f}}_t$ [N] | **Indentation Velocities** [mm/s] | | | |
|---|---|---|---|---|
| | ***4*** | ***8*** | ***12*** | ***16*** |
| **8%** | **0.41±0.02*** | 0.50±0.02 | 0.52±0.01 | 0.57±0.03 |
| **12%** | 0.78±0.02 | 0.96±0.03 | 1.08±0.01 | 1.14±0.05 |
| **16%** | 1.04±0.03 | 1.27±0.05 | 1.42±0.03 | 1.44±0.04 |
| $\overline{p}_t$ [mm] | **Indentation Velocities** [mm/s] | | | |
| | ***4*** | ***8*** | ***12*** | ***16*** |
| **8%** | **5.49±0.28*** | 6.28±0.39 | 6.38±0.17 | 6.34±0.43 |
| **12%** | 5.33±0.14 | 6.06±0.19 | 6.43±0.15 | 6.46±0.38 |
| **16%** | 5.52±0.22 | 6.36±0.25 | 6.75±0.17 | 6.67±0.14 |

(*) critical tool insertion scenario reporting the minimum puncturing force

The median value and the first and third IQRs of the puncturing forces and the correspondent penetration level among trials are reported in Table 3.1. A safety level for each different gelatin concentration is identified according to the minimum puncturing force (0.4N with 8%, 0.7N with 12%, 1N with 16%).

### 3.2.2.2 Optimization of the FFE controller

The force feedback enhancement loop was optimized considering the critical tool insertion scenario (8% gelatin at 4mm/s), which reports the minimal puncturing force (mean value 0.41N at ≈5.5mm mean penetration) (Table 3.1). The FFE parameters ($n$, $\rho$)

were tuned so that the user was able to perceive contact when the tissue reacts with a force equal to a percentage ($\lambda$) of the critical puncturing force, considered as a safety margin. The minimum user perceivable force ($\underline{\mathbf{f}}_h$) during assisted targeting tasks is strictly related to the static friction of the system (±1.5Nm internal thresholds on the robot joint torque sensors) and varies along the workspace according to the robot configuration (up to 3N). It was considered equal to 4N.

After limiting the non-linear characteristic of the enhancement (*n* set to 0.8) and considering a safety margin of 50% ($\lambda$=0.5), the amplitude parameter, ρ, was computed as:

$$\rho = \frac{\underline{\mathbf{f}}_h}{\left(\lambda \bar{\mathbf{f}}_t\right)^n} \tag{3.8}$$

and accordingly set to 14.5. The saturation force $\mathbf{f}_s$ was set equal to 10N.

### 3.2.2.3 Evaluation of the FFE controller performance

During targeting an arbitrary point of the gelatin surface was approached and the pose was held for 2s. The users were asked to keep contact with the tissue during the interaction, preventing unwanted gelatin damage.

The effectiveness of the proposed FFE loop was comparatively assessed during repetitive targeting tasks on a pool of 6 non-expert users. Every user performed 8 targeting gestures in a randomized order on 8%, 12% and 16% gelatin samples in these modalities:

- Freehand (FH): the targeting task was performed with an optical pointer (3mm diameter tip); the pencil-style hand grip is equal to the standard bipolar stimulator tools;
- Robotic assistance (RA) without force feedback ($n$=0; $\rho$=0);
- Robotic assistance with force feedback enhancement loop (FFE) ($n$=0.8; $\rho$=14.5).

In both the robotic assistive cases (RA and FFE), the user performed the targeting tasks guiding the 3 translational DoFs of the manipulator, while the orientation of the tool was fixed to an initial configuration. During each trial, the force and TCP position signals were processed, in order to detect the beginning/end of the holding phase during the tool-tissue contact. The following indexes of performance were evaluated for each trial:

- Execution time ($T$): computed from the moment in which the TCP is close 5cm to the surface to the identified initial time of the holding phase;
- Mean holding force ($F_H$): computed as the mean force of the load cell measurements ($\mathbf{f}_{lc}$) during the holding phase;
- Mean holding penetration ($P_H$): computed as the mean signed distance of the TCP position ($\mathbf{t}_{tcp}$) from the registered surface (positive values refers to position below the surface, thus indentation depths) during the holding phase;
- Amplitude variability of the force/penetration ($V_F$ /$V_P$): computed as the root mean square (RMS) distance from the mean values ($F_H$ and $P_H$ respectively) during the holding phase.

The median value and the first and third IQRs were computed over different trials and different users for $T$, $F_H$ and $P_H$ indexes. A comparative analysis of the different task execution modalities (FH, RA, FFE) and of the different tissue's mechanical properties (8-16% gelatin concentration) was carried out using the Kruskal-Wallis test with Bonferroni-Holm correction ($p<0.05$) (Holm, 1979). The amplitude variability indexes ($V_F$ and $V_P$) were computed over trials of each user in each execution modality (FH, RA, FFE) and for each gelatin concentration (8%,12%,16%).

## 3.3 Results

The analysis performed on the execution time ($T$) index during the indentation phase is reported in Table 3.2. The execution time computed for the RA (medina time below 3s) and FFE (median time below 2.5s) modalities resulted significantly greater than the one required to execute the task in FH mode (median time below 1.3s) for each experimental conditions. No statistically significant difference was reported between the RA and FFE modes.

The results of the comparative analysis performed on the mean holding force ($F_H$) and penetration ($P_H$) indexes are reported in Figure 3.4. The forces $F_H$ resulted significantly smaller when the task is executed in FFE mode (75% quartile value below the 0.2N perception threshold) with respect to both FH and RA modes with all the gelatin phantoms.

**Table 3.2** Time Execution index

| *T* [s] | Task Execution Modalities | | |
|---|---|---|---|
| | ***FH*** | ***RA*** | ***FFE*** |
| **8%** | 1.32 ± [0.60; 0.25]* | 2.68 ± [0.93; 0.81] | 2.54 ± [0.83; 1.65] |
| **12%** | 0.83 ± [0.35; 0.49]* | 2.87 ± [1.16; 1.47] | 2.02 ± [0.65; 1.11] |
| **16%** | 0.74 ± [0.44; 0.43]* | 2.61 ± [0.50; 0.68] | 2.42 ± [0.55; 1.46] |

(*) statistically significant difference

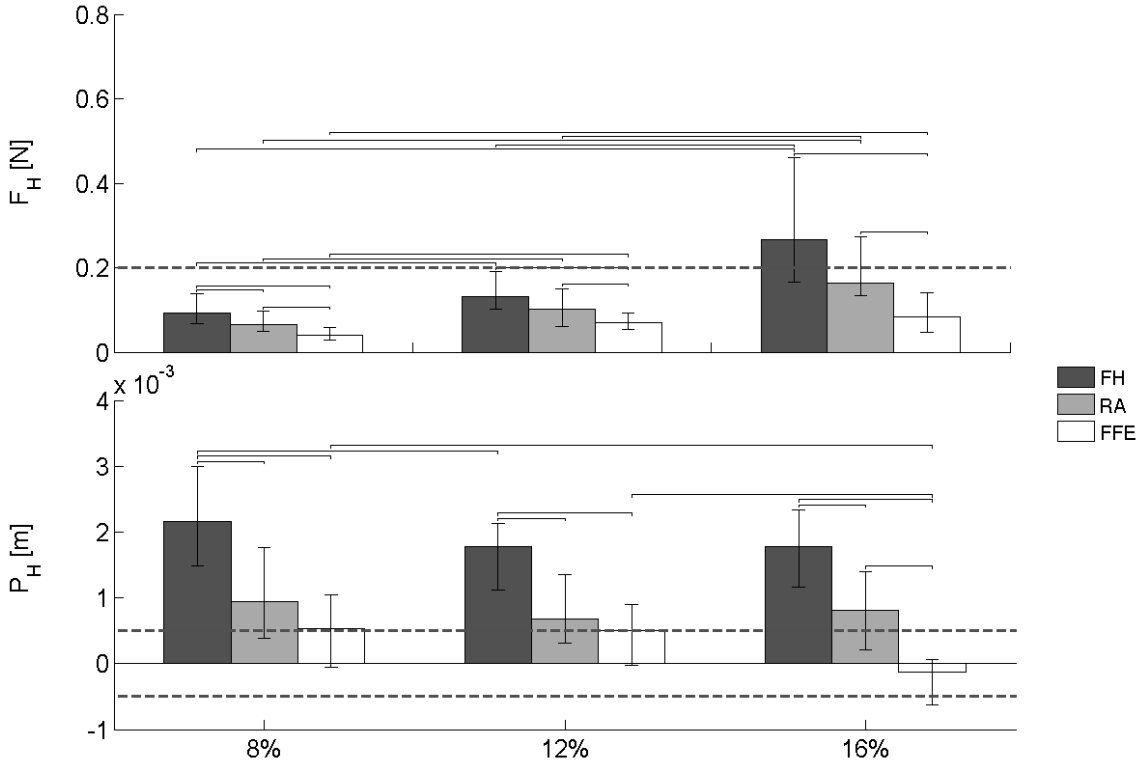


**Figure 3.4** Evaluation of the holding force $F_H$ and penetration $P_H$ indexes using the three task execution modalities (FH, RA, FFE) and the three different concentration gelatin phantoms (8%,12%,16%), for all trials of the 6 non-expert users. Vertical bars represent median values and quartiles (25% and 75%) of performance index population. Horizontal lines represent statistically significant differences as determined in intra-group and inter-group comparisons (Kruskal-Wallis test, $p<0.05$) with Bonferroni-Holm correction. Also, the force safety margin used to compute the optimal FFE control parameters (0.2N) and the surface registration error threshold (0.5mm) are reported (horizontal dot lines).

While the comparable forces computed in FH (median value above 0.25N) and RA (median value above 0.15N) modes significantly increased according to higher gelatin concentrations, no statistically significant difference was computed between the 12% and 16% gelatin phantoms in FFE mode. The $F_H$ indexes resulted below the identified safety level for the different gelatin concentration (0.4N with 8%, 0.7N with 12%, 1N with 16%).

Accordingly, the holding penetration depth ($P_H$) during FH task executions (median value above 1.5mm) resulted significantly greater with respect to RA (median depth in the range (0.5-1) mm) and FFE (median depth below 0.6mm) modes. No statistically significant differences are computed among the penetration depths on gelatin phantoms with different concentrations both for the FH (except for the comparison between 8% and 12 % gelatins) and RA modes. Conversely, the penetration depths on 16% gelatin during FFE task executions resulted significantly smaller than the other cases. In this case, the depth values are below the 0.5mm surface registration error.

As reported in Table 3.3, the amplitude variability computed among users on the force ($V_F$) and penetration depth ($V_P$) signals during the holding phases in the assisted task executions (RMS error below the accuracy of the measurement systems, 0.02N and 0.1mm respectively) resulted significantly reduced by a factor of 10 with respect to the freehand modality (RMS error up to 0.13N and 0.8mm respectively).

**Table 3.3** Amplitude Variability analysis among trials and users

| $V_P$ [mm] | **Task Execution Modalities** | | |
|---|---|---|---|
| | ***FH*** | ***RA*** | ***FFE*** |
| **8%** | 0.8* | <0.1 | <0.1 |
| **12%** | 0.6* | <0.1 | <0.1 |
| **16%** | 0.6* | <0.1 | <0.1 |
| $V_F$ [N] | **Task Execution Modalities** | | |
| | ***FH*** | ***RA*** | ***FFE*** |
| **8%** | 0.04* | <0.02 | <0.02 |
| **12%** | 0.06* | <0.02 | <0.02 |
| **16%** | 0.13* | <0.02 | <0.02 |

(*) the assumption ($V_{FH} > V_{RA}$) and ($V_{FH} > V_{FFE}$) is verified for all samples.

## 3.4 Discussion

In order to enhance the human-robot cooperation during targeting tasks on soft tissues in surgery, such as during brain cortex stimulation procedures in open-skull neurosurgery, a torque controller with non-linear force feedback (FFE) is proposed. The controller provides enhanced haptic perception to the operator when the surgical tool is in contact with the soft tissue. In fact, such contact forces between the surgical tool and the soft tissues, e.g. brain (0.03-0.3N (Paragraph 1.2.1)) and/or liver (peak forces below 1N (Maurin et al. 2004)), are too small to be perceived by the user during the robotic guidance, due to the residual inertia and friction of the manipulator (Marayong et al. 2006). Differently from vitro-retinal surgery (Uneri et al. 2010) (MacLahlan et al. 2012) and/or needle insertion procedures (De Lorenzo, Koseki et al. 2013), in which the accuracy requirements are very high demanding in a constrained and limited working space, force-to-motion control schemas may be not the best suited solution for wide motion targeting tasks, e.g. brain cortex stimulation (Paragraph 1.4). The proposed approach is based on a high compliant cooperative control with a force feedback augmentation strategy, to augment the surgeon's ability in performing a safe and stable contact with the soft tissue.

To comparatively assess the performance of the proposed FFE controller in a controlled and repeatable setup, tests were performed using gelatin phantoms at different concentrations (8-16%), where the 8% concentration gelatin is reported to better represents the viscoelastic properties of the brain (De Lorenzo et al. 2011). Strictly dependent on the tool shape, geometry and the tool insertion velocity (Abolhassani et al. 2007), the puncturing forces measured during the gelatin characterization protocol resulted consistent to the ranges reported in in-vivo studies (Wittek et al. 2008) (Maurin et al. 2004), increasing with respect to gelatin concentration. Accordingly, a safety force criterion was considered to evaluate the tissue's damage during indentation, depending on the concentration of each gelatin phantom (0.4N with 8%, 0.7N with 12%, 1N with 16%).

The FFE controller proved to significantly reduce the amount of forces applied to the tissue during indentation with respect to both the freehand execution and the robotic assistance without force enhancement, as shown by the holding force index $F_H$ (Figure 3.4).

During FH and RA task executions, the users reach the contact equilibrium using pure visual feedback information, as proved by comparable holding penetration depths (median $P_H \approx 2$mm in FH and median $P_H \approx 1$mm in RA) among different concentration gelatin phantoms. Conversely, during FFE task execution, the effect of the haptic feedback provided to the user is shown by comparable tissue's interaction forces ($F_H \approx 0.1$N) for the 12% and 16% gelatin phantoms. In fact, the indentation level during contact with the 16% gelatin is reduced below the registration accuracy of the phantom's surface (0.5mm), thus it can be considered negligible. Although the mean holding forces applied by the users in each experimental condition were below the identified safety levels for each task execution modes and no tissue's penetration were registered, the indentation with FFE was significantly reduced.

Besides the fact that the execution time in RA and FFE resulted slightly increased with respect to FH execution modality (as shown in Table 3.2), the use of a robotic assistant was proved to highly reduce the tremor of the hand during the instrument holding phase, allowing for a more stable contact with respect to freehand task execution, as shown by a 10 factor reduction of the $V_P$ index in FH (≈1mm) with respect to RA and FFE modes (<0.1mm) reported in Table 3.3. The estimate of the hand tremor during contact resulted greater than other studies for microsurgery (Sandoval et al. 2007), but it has to be noted that the users were asked to perform the targeting tasks while standing, without arm support and without magnification, in order to be comparable to the tasks execution with robotic assistance. Indeed, the hand tremor resulted comparable with values reported for the same experimental conditions in (Safwat et al. 2009).

In this work, the non-linear characteristic of the FFE controller was optimally tuned based on a predefined safety margin (50% of the critical puncturing force), which strictly depends on the mechanical characteristics of the specific tissue, and set constant during the contact. In order to generalize the approach to softer/harder tissues, an adaptive criterion based on the online estimate of the tissue's stiffness should be added to the FFE controller.

In conclusion, non-linear force feedback torque control was presented and experimentally evaluated on a flexible joint redundant manipulator to provide enhanced haptic perception

during cooperatively assisted targeting tasks in surgery. The FFE controller was proved to allow for a stable, i.e. reduction of the free-hand tremor by a factor of 10 during the holding phase, and safe, i.e. 50% reduction of the indentation level, contact with the tissues.

# Chapter 4

# Brain cortex stimulation: a feasibility study[4]

This chapter presents a feasibility study aimed at investigating the applicability of two torque-based impedance control approaches to cooperatively assist the surgeon during open-skull brain cortex stimulation procedures: the space variable damping criterion (presented in Chapter 2) and the non-linear force feedback control (presented in Chapter 3). Singularly and combined, the proposed controllers were tested by naive users and neurosurgeons on brain-mimicking phantoms in a realistic intraoperative surgical scenario for brain cortex stimulation. Their performances were evaluated, both quantitatively and qualitatively, with respect to the state-of-the-art admittance controller (Lawrence, 1988) and to the free-hand task execution, assessing the respect of the clinical requirements (Paragraph 1.2.1).

## 4.1 Material and Methods

A Cartesian torque-based impedance controller (Albu-Schäffer et al., 2004) was implemented for the 7 DoFs lightweight robot LWR4+ (characteristics reported in Paragraph 2.2.4). In order to manage the kinematic redundancy, the Cartesian impedance controller is combined with a damped posture strategy with hierarchical task prioritization approach (Sentis and Khatib, 2005)(see Paragraph 2.2.1). The two independent modulation criteria proposed to enhance the performance of assisted targeting tasks on soft tissue are represented in Figure 4.1:

- *space variable damping criterion (SV)* (Paragraph 2.2.3): the viscosity of the impedance-controlled manipulator is modulated according to the position of the

[4] A journal paper on this work has been submitted as **Beretta E**, Nessi F, Ferrigno G, DiMeco F, Perin A, Bello L, Cardinale F, De Momi E. Enhanced torque-based impedance control to assist brain targeting during open-skull neurosurgery: a feasibility study.

stimulation target: higher damping is achieved only in areas of the robot workspace where high positional accuracy is required;

- *force feedback enhancement criterion (FFE)* (Paragraph 3.2.1): the interaction forces generated by the contact with the soft tissue during the surgical tool placement, which may be masked by the residual inertia and friction of the manipulator, are increased to provide enhanced haptic perception to the user.

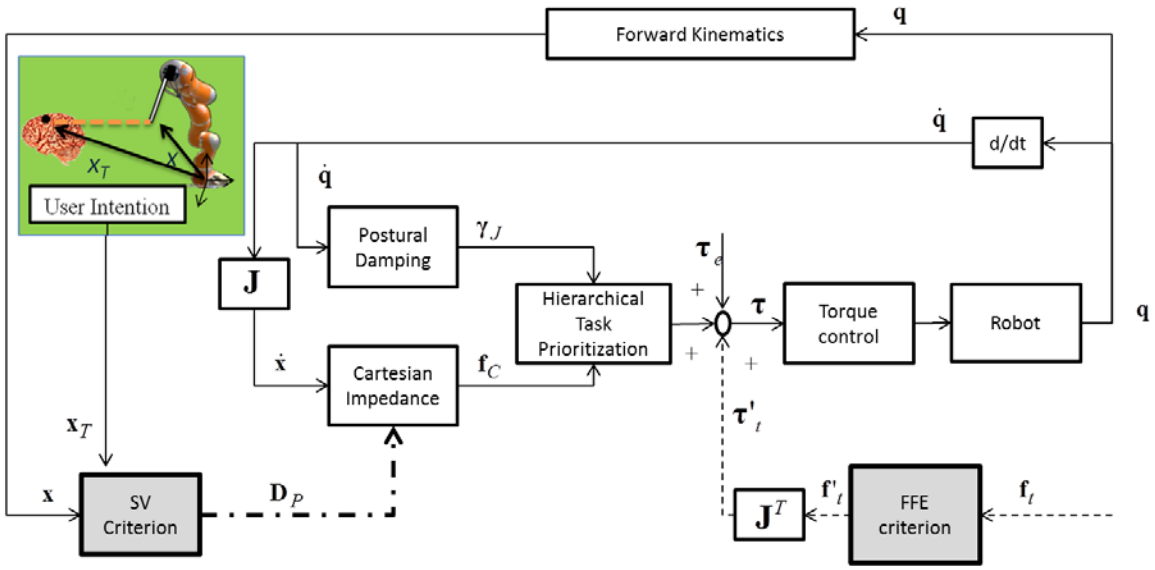


**Figure 4.1** Scheme of the torque-based impedance controller. The hierarchical task prioritization approach combines the commands computed with the Cartesian impedance controller ($\mathbf{f}_C$) with the postural damping commands ($\gamma_J$) in the joint space. The actual Cartesian linear velocities $\dot{\mathbf{x}}$ are computed from the actual joint velocities $\dot{\mathbf{q}}$ with the geometrical Jacobian **J**. Both the Space Variable damping (SV) and the Force Feedback enhancement (FFE) criteria are reported. The SV criterion (bold dot line) varies the Cartesian translational damping parameter ($\mathbf{D}_P$) depending on the actual position of the control point (**x**) and on the known position of the target ($\mathbf{x}_T$). The FFE criterion (dot line) computes the augmented Cartesian forces ($\mathbf{f}'_t$) based on the soft tissue's force measurements ($\mathbf{f}_t$), then converted into torques ($\boldsymbol{\tau}'_t$) with the transpose of the geometrical Jacobian. $\boldsymbol{\tau}_e$ is the vector of the external torques applied to the manipulator by the environment, due to the human guidance force and the tissue' contact (Paragraph 3.2.1). The feed forward torques for the compensation of the robot's dynamic are not reported.

### 4.1.1 SV criterion

The SV criterion (Paragraph 2.2.3) encompass an isotropic sigmoid-shape modulation of the independent damping parameters of the manipulator based on the position of the surgical target (Figure 4.1). Nevertheless, during brain cortex stimulation in neurosurgery, the stimulation site on the exposed brain cortex is not known *a priori* in the pre-operative phase and changes its position during the procedure depending on the surgeon's stimulation intentions. Thus, an image-guided navigation system is proposed for the application of the SV controller during brain mapping procedures, with which the surgeon is able to configure the damping field online, based on his/her actual intention of motion. In particular, the position of the intended surgical target ($\mathbf{x}_T$) can be intra-operatively acquired using the robot arm as a navigation tool.

In this work, the SV criterion was applied only on the translational damping parameters ( $\mathbf{D}_P$ ), while virtual constraints were imposed on the rotation of the end-effector. The lower damping boundary was set null ($\underline{\mathbf{D}}_P = 0 Ns/m$) to allow the most transparent interaction with the user, while the upper damping boundary mimics the human arm damping effect ( $\overline{\mathbf{D}}_P = 30 Ns/m$) (Paragraph 2.2.4). The spatial parameters of the SV criterion were heuristically determined ($m$=30mm and $\beta$=70m$^{-1}$) based on the qualitative considerations of a naive user during the repetitive execution of targeting gestures on a predefined known target.

### 4.1.2 FFE criterion

The measured soft tissue interaction forces ( $\mathbf{f}_t$ ) are augmented with the non-linear force feedback enhancement (FFE) criterion (Figure 4.1)(Paragraph 3.2.1). The tuning of the FFE parameters was performed as in Chapter 3, taking into account a minimum user perceivable force equal to 4N, a safety margin of 50% and the non-linear characteristic of the enhancement ($n$ = 0.8). The saturation force ( $\mathbf{f}_s$ ),which defines the maximum tissue force fed back to the user, thus representing the maximum force the user has to overcome to intentionally penetrate the tissue, was 10N.

### 4.1.3 Space variable criterion with force feedback enhancement (SVFFE)

Both the SV damping and the FFE criteria were combined in the space variable damping with force feedback enhancement (SVFFE) controller. Thanks to the fact that the two modulation approaches operate on different control parameters, their effects can be linearly combined to compute the commanded torque ($\boldsymbol{\tau}$), as shown in Figure 4.1.

### 4.1.4 Preparation of brain-mimicking phantoms

Gelatin is commonly used to model brain tissues (Parittotokkaporn et al. 2008), due also to the fact that the material properties can be tuned varying the water concentration in the solution, prior to solidification. Having mechanical properties similar to in-vitro swine brain (Miller et al. 2000) during indentation (De Lorenzo et al. 2011) and insertion (Ritter et al. 1998), gelatin phantoms with 8% concentration were used. The gelatin was stored in a refrigerator for at least eight hours at 5° before its usage. For each subject who performed the experiments, a brand new gelatin preparation was used, in order to avoid degradation of the shape and of the mechanical properties and to standardize the material characteristics.

A 8x3 grid of circular points (10mm distance ($d_s$), 3mm diameter ($d_m$)) was drawn on the surface of each gelatin phantom using colored ink, representing the stimulation targets. Six additional points were also placed as calibration divots for the image-based navigation system. In order to place the points in *a priori* known positions, a syringe (0.7mm diameter of the needle) was rigidly attached in a vertical configuration to a PowerWasp EVO CNC machine (WASProject, Ravenna, Italy)(0.1mm accuracy). The needle's tip was automatically moved along the horizontal plane 2mm away from the gelatin surface, starting from an arbitrary initial position, and an ink drop was manually pushed out for each target. The accuracy of this semi-automatic process was measured a-posteriori. An high-resolution Digital Single-Lens Reflex camera was perpendicularly placed at about 40cm distance from the gelatin surface using a spirit level, in order to avoid both visual perspective effects. The positions of the centroids of the grid points were computed using the Image Processing Toolbox™ (Matlab R2014b, Mathworks, Natick, MA) applying the

following steps: 1) contrast enhancement and binary conversion; 2) binary erosion and dilatation processes using a 4-connectivety circular structuring element (7px and 15px diameters respectively), to better define the segmented region's contours; 3) extraction of the centers of mass of each connected region of the binary image, representing the centroids of the target grid. The centroids' grid extracted in the image space is registered to the ideal target grid in the 3D space through a non-correspondent iterative closest point algorithm (Besl and McKay, 1992).

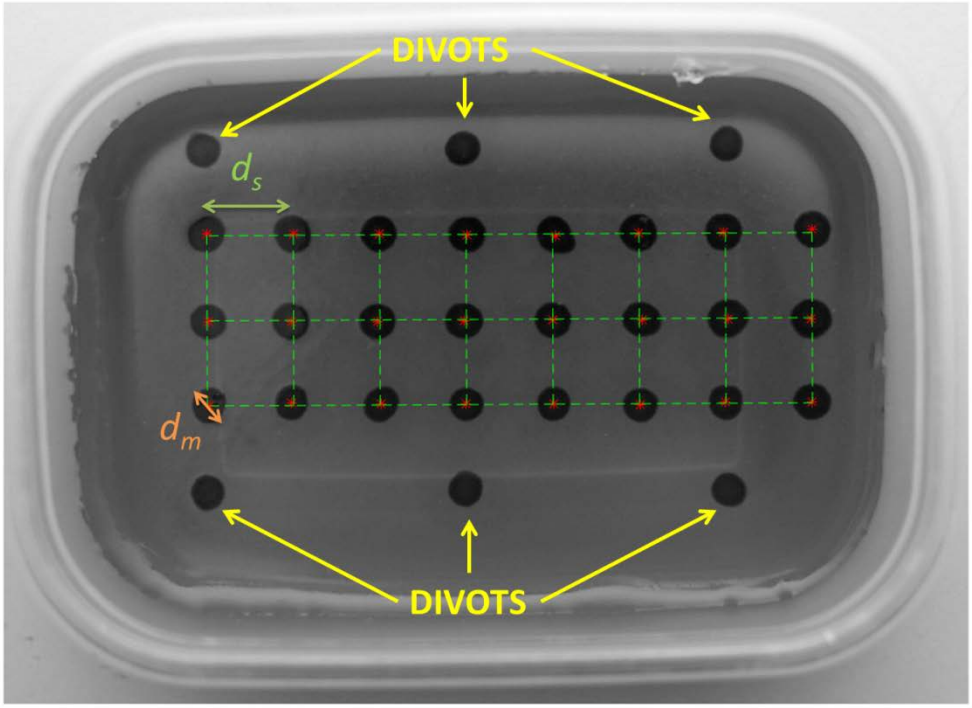


**Figure 4.2** Example of the accuracy evaluation of the target placement process on a gelatin phantom. The grayscale conversion of the blue channel image derived from the original high-resolution picture is shown. The extracted centroids of each target (red markers) and the registered grid of the ideal targets (green lines) are represented. The target diameter ($d_m$) and the distance between consecutive targets on the grid ($d_s$) are also shown together with the six calibration divots.

First, the scaling factor ($s$), which was the ratio between the ideal distance in the 3D space ($d_s$) and the minimum distance computed between couple of centroids ($C_i$,$C_j$) in the image space, was computed and applied to the centroids dataset:

$$s = \frac{d_s}{\min(\|C_j - C_i\|)} \qquad i, j = 1,...,24 \qquad i \neq j \qquad (4.1)$$

Then, the correspondent points of the ideal grid and the centroids' grid were registered with an overdetermined Helmert affine 2D transformation (Watson, 2006), as shown in Figure 4.2. The RMS error between the registered image-extracted centroids and the ideal points resulted inferior to 0.3mm for all the gelatin phantoms used in the experiments, thus defining the overall accuracy of the system.

### 4.1.5 Experimental setup

The experimental setup used in this work is the same as one presented in Paragraph 3.2.2, including the 7 DoFs LWR with a Nano43 F/T sensor placed at the end-effector, a Gamma F/T sensor placed below the gelatin phantom and the Optotrack Certus localization system. The tool tip position ($\mathbf{t}_{tcp}$) and the force measurements of the load cell ($\mathbf{f}_{lc}$) were computed in the reference frame defined on the the gelatin plate ($\mathbf{RF}_P$) (Paragraph 3.2.2). The surface of each gelatin phantom was obtained in $\mathbf{RF}_P$, acquiring the position of the six gelatin divots with the optically tracked robotic arm.

The image-based navigation system was developed in the open-source 3D Slicer environment (Fedorov et al. 2012), in which a 3D model of the gelatin phantom was built (Figure 4.3). The gelatin target's grid was calibrated in the image space through the corresponding point registration procedure (Horn, 1987) using the acquired position of the six gelatin divots. A custom defined Graphical User Interface (GUI) allowed to configure online the SV damping field, acquiring the intended stimulation target ($\mathbf{x}_T$) as the position the point which is 5cm away along the tool $z$-axes from the current TCP pose. It displays the forces due to the tissue's interaction and record the positions of the stimulation points ($\mathbf{t}_s$).

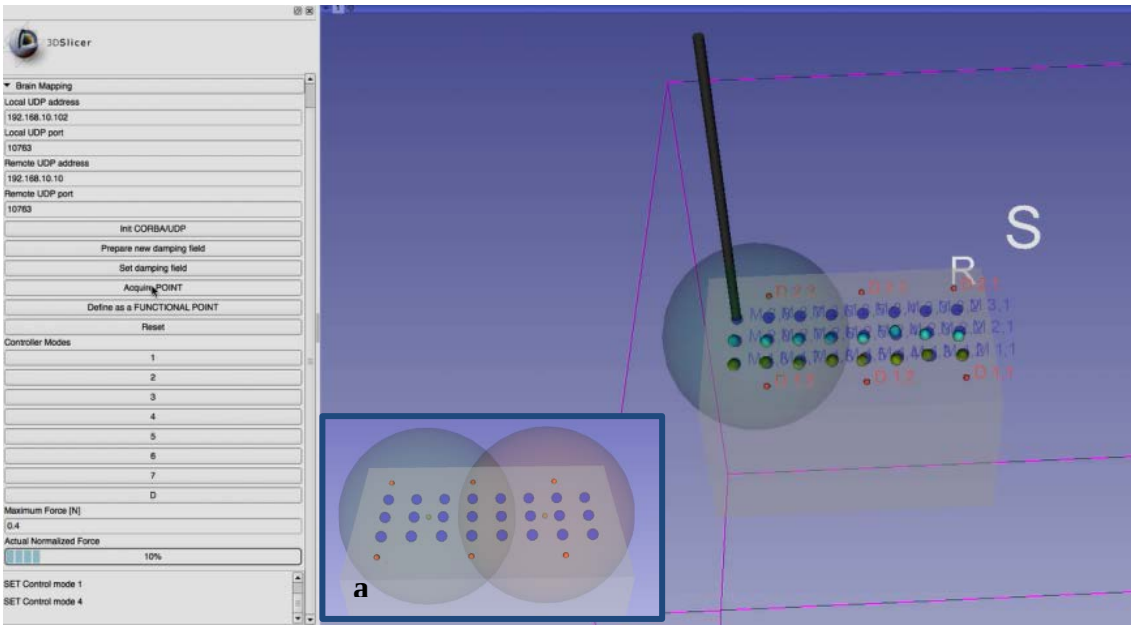


**Figure 4.3** Image-based navigation system. The calibrated gelatin phantom is shown together with the current pose of the tool (gray cilinder), the current SV damping field (semi-transparent sphere) and the previously acquired stimulation targets (coloured fiducials). The GUI includes buttons for the online configuration of the damping field, the acquisition of the stimulation points and the progress bar to display the current interaction forces with the tissue. a) the two damping field configure during the SV modulation criteria for the experiments #1, #2, #3.

### 4.1.6 Design of Experiments

In order to evaluate the performance of the two modulation criteria proposed, five cooperative robotic control modalities were used in the experiments:

- Gravity compensation (GC) robotic assistance, i.e. the manipulator was controlled with a zero impedance behavior ($\underline{\mathbf{D}}_P = \overline{\mathbf{D}}_P = 0Ns/m, \rho = 0$), in order to evaluate the maximum transparency of the system; none of the modulation criteria was enabled.
- Space variable impedance (SV) robotic assistance; the SV modulation criterion was enabled ($\underline{\mathbf{D}}_P == 0Ns/m, \overline{\mathbf{D}}_P = 30Ns/m, \rho = 0$) with two damping fields *a priori* configured on the calibrated gelatin phantom, covering the grid of targets (as in Figure 4.3a);

- Constant low impedance robotic assistance with force feedback enhancement (FFE); the FFE criterion was enabled ($\underline{\mathbf{D}}_P = \overline{\mathbf{D}}_P = 0 Ns/m, \rho = 14{,}5$) and the amplitude parameter was computed according to the minimal puncturing force (0.4N) for an 8% concentration gelatin (Paragraph 3.2.2.1);
- Space variable impedance robotic assistance with force feedback enhancement (SVFFE); both the SV and FFE modulation criteria were enabled ($\underline{\mathbf{D}}_P == 0 Ns/m, \overline{\mathbf{D}}_P = 30 Ns/m, \rho = 14{,}5$);
- Constant high admittance robotic assistance with force feedback enhancement (ADM); the admittance controller was implemented as a proportional control (Lawrence, 1988) and combined with the proposed FFE controller ($\rho = 14.,5$); the proportional gain was experimentally optimized to obtain the maximum compliant stable behavior during free-motion guidance, resulting in a constant virtual damping ($300 Ns/m$) 10 times higher than the upper boundary of the SV damping parameter ($\overline{\mathbf{D}}_P = 30 Ns/m$).

The subjects were asked to grasp the handle attached on the manipulator with their dominant hand and guide the tool towards brain-mimicking gelatin phantoms, while standing and without any arm support. The task consisted in 1) *approaching* phase, i.e. positioning the tip of the tool in contact with the surface of the gelatin phantom on a marker, limiting the indentation of the soft tissue as much as possible (a tiny and gentle surface deformation was allowed); 2) *holding* phase, i.e. maintaining the contact for at least 2s, as in standard protocols (Szelènyi et al. 2010), while giving a vocal command for the acquisition of the stimulation point ($\mathbf{t}_{sp}$) with the image-based navigation system. The subjects were instructed to pull the tool away from the gelatin phantom (at least 10cm away from the surface) after each targeting task.

The subjects were also asked to perform the task described above in free-hand mode (FH), using an optical pointer (3mm diameter tip), whose pencil-style hand-grip is equal to the standard bipolar stimulator tools. Differently from the robotic assistance modalities, the subject was asked to perform the task with arm support while standing, in order to mimic the operating room conditions.

Visual feedback on the tool and gelatin phantoms was provided to the subject during the experiments. No information on the control modalities was provided, neither of their nature nor on the particular order with which they were going to be presented to the subject. The sequence of the control modalities was randomized. The image-based navigation system was used to acquire the stimulation points during the holding phase.

The experiment consisted in repeating the targeting task (described above) 8 time consecutively, for each different cooperative robotic control modes and for the free-hand mode. The following subjects took part in the experiment:

- Thirteen naive users (N) (5 male and 8 female, age 23-31). Four of them had previous experience with robotic system. None of the participants reported any deficiencies in the perception abilities;
- Eight neurosurgeons, i.e. four novices (NS) (males, age 26-35) and four experts (ES) (males, age 42-50), took part in the experiment. Previous experience with robotic system is reported in Table 4.1.

#### 4.1.6.1 Performance indexes

During each trial, the force ($\mathbf{f}_{lc}$) and TCP position ($\mathbf{t}_{tcp}$) signals were acquired. The penetration signal ($p_{tcp}$) was computed as the signed distance of the TCP position ($\mathbf{t}_{tcp}$) from the calibrated gelatin surface (positive values refers to position below the surface, thus indentation depths) (Figure 4.4). The beginning of the approaching phase ($t_{A,0}$) was the time instant in which the TCP is at a fixed distance (M=8cm) from the phantom surface. The end of the approaching phase ($t_{A,N}$) was the beginning of the holding phase. The beginning ($t_{H,0}$) and the end ($t_{H,N}$) of the holding phase were identified for each trial with an automatic threshold procedure along the norm of $\mathbf{f}_{lc}$ signal. The time derivatives of the Cartesian TCP position ($\mathbf{t}_{tcp}$) were computed with a best-fit First Order Adaptive Window Recursive filter (Janabi-Sharifi et al. 2000). The following indexes of performance were evaluated for each trial in the identified time phases:

**Table 4.1** Features of the enrolled neurosurgeons, divided between experts (ES) and novices (NS).

| | **Yp**[1] | **P/y**[2] | **E**[3] | **DH**[4] | **RS**[5] | **NS**[6] | **PP**[7] |
|---|---|---|---|---|---|---|---|
| **ES1** | 19 | 200 | Surgery of intracranial tumor, mainly glioma located in eloquent areas | B | N | Y | St,wo |
| **ES2** | 17 | 40 | Epilepsy surgery (resection) | R | Y | Y | Si,w |
| **ES3** | 12 | 200 | Surgery of intracranial tumor | R | Y, training with haptic simulator | Y, always | St, w |
| **ES4** | 20 | | Surgery of intracranial tumor | R | Y, training with haptic simulator | Y | St, w |
| **NS1** | 0 | 0 | - (first year of specialization) | R | N | N | - |
| **NS2** | 6 | 40 | Epilepsy surgery (resection) | R | Y, intracranial electrodes placement | Y, biopsy | Si,w |
| **NS3** | 5 | 5 | Epilepsy surgery (resection) | R | Y, intracranial electrodes placement | Y, biopsy | Si,w |
| **NS4** | 2 | 30 | Ipotalamic lesion disconnection | L | Y, SEEG, endoscopy and biopsy | Y, tumor resection | St, w |

[1] Years in practise (**Yp**)
[2] Procedures performed per year (**P/y**)
[3] Main area of expertise (**E**)
[4] Dominant Hand (**DH**): left-handed (L)/ right-handed (R)/ both (B)
[5] Previous experience with robotic systems (**RS**)
[6] Previous experience with navigation systems (**NS**)
[7] Preferred position (**PP**): Standing (St)/Sitting (Si), with(w)/without(wo) arm rest

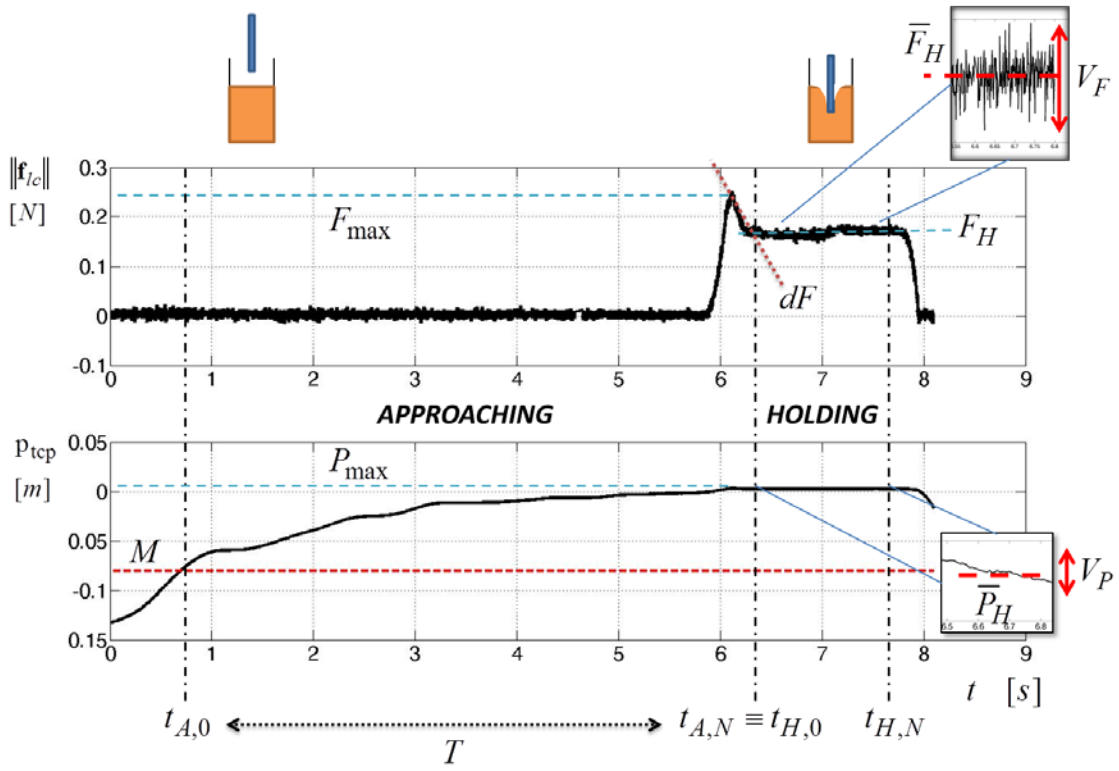


**Figure 4.4** Example of force ($\mathbf{f}_{lc}$) and penetration ($p_{tcp}$) signals computed on a targeting task trial performed by a naive user. The initial and final time sample of the approaching ($t_{A,0}$ and $t_{A,N}$) and holding phases ($t_{H,0}$ and $t_{H,N}$) are shown together with the *approaching* execution time index ($T$) and the *global* performance indexes: maximum applied force ($F_{max}$), maximum penetration level ($P_{max}$) and force slope ($dF$). The amplitude variability indexes on force ($V_F$) and penetration ($V_P$) computed with respect to the mean force ($\overline{F}_H$) and penetration level ($\overline{P}_H$) in the holding phase are also reported.

Approaching indexes (A, $t = t_{A,0}, \ldots, t_{A,N}$):

- execution time index ($T$), computed as the difference between $t_{A,N}$ and $t_{A,0}$, as shown in Figure 4.4;
- guidance force index ($F_g$), computed as the mean norm of the exerted Cartesian forces at the end-effector ($\mathbf{f}_e$), in order to quantify the transparency of the system and thus the user's efforts during the cooperation;
- acceleration index ($Acc$), computed as the maximum norm of the TCP acceleration ($\mathbf{a}_{tcp}$), i.e. second discrete time derivative of the TCP position ($\mathbf{t}_{tcp}$);

- zero crossing index ($ZC_a$) of the TCP acceleration signal ($\mathbf{a}_{tcp}$), in order to quantify the number of velocity changes experienced while approaching the target;
- motion smoothness index ($S$) (Teulings et al. 1997), computed as the root mean square integral jerk, i.e. third discrete time derivative of the TCP position ($\mathbf{t}_{tcp}$):

$$S = \sqrt{\frac{1}{3}\sum_{i=t_{A,0}}^{t_{A,N}} \left\| \left( \frac{d^3 \mathbf{t}_{tcp}}{dt^3} \right)^i \right\|^2 \frac{T^5}{L^2}} \tag{4.2}$$

  where $T$ and $L$ are normalization factors, respectively equal to the trajectory duration and the trajectory length. $L$ is computed as the discrete integral of the averaged (10 samples) TCP position ($\mathbf{t}_{tcp}$).

Holding indexes (H, $t = t_{H,0}, \ldots, t_{H,N}$):

- amplitude force variability ($V_F$): RMS distance of the force signal ($\mathbf{f}_{lc}$) from the mean force ($\bar{\mathbf{f}}$), computed as:

$$V_F = \sqrt{\frac{1}{N}\sum_{i=t_{H,0}}^{t_{H,N}} \left\| \mathbf{f}_{lc}^i - \bar{\mathbf{f}} \right\|^2} \tag{4.3}$$

  where $N$ is the number of time sample of the holding phase;

- amplitude penetration variability ($V_P$): RMS distance of the penetration signal ($p_{tcp}$) from the mean penetration ($\bar{p}$), computed as:

$$V_P = \sqrt{\frac{1}{N}\sum_{i=t_{H,0}}^{t_{H,N}} \left| p_{tcp}^i - \bar{p} \right|^2} \tag{4.4}$$

Global indexes (G, $t = t_{A,0}, \ldots, t_{H,N}$):

- target pointing error ($E_T$), computed as the distance between the known target position ($\mathbf{t}_{gs}$, gold standard) and the acquired stimulation target position ($\mathbf{t}_s$) projected on the gelatin surface:

$$E_T = \left\| (\mathbf{t}_s - \mathbf{t}_{gs}) - ((\mathbf{t}_s - \mathbf{t}_{gs}) \cdot \mathbf{n}_s)\mathbf{n}_s \right\| \tag{4.5}$$

  where $\mathbf{n}_s$ is the versor perpendicular to the gelatin surface plane;

- maximum force applied to the tissue ($F_{max}$), computed as the maximum norm of the force signal ($\mathbf{f}_{lc}$) along the trajectory;
- maximum penetration ($P_{max}$), computed as the maximum value of the penetration signal ($p_{tcp}$) along the trajectory;
- indentation force slope ($dF$), computed as:

$$dF = \frac{\left\|\bar{\mathbf{f}}\right\| - F_{\max}}{t_{H,0} - t\big|_{\mathbf{f}_{lc}=F_{\max}}} \tag{4.6}$$

  in order to detect overshooting on force signal ($\bar{\mathbf{f}} < F_{\max}$, negative slopes) during the tissue's indentation.

#### 4.1.6.2 Performance analysis

Three experiments were performed, as summarized in Table 4.2:

*experiment #1: evaluate the ability of maintaining the tool in a stable position during tissue's contact.* The *holding* performance of N, NS and ES users were computed during free-hand execution and compared to the robotic assisted modes. This comparison aimed at confirming that an assisted device can limit the hand tremor and positioning variability occurring during the free-hand task executions (MacLachlan et al. 2012). Moreover, the analysis allowed verifying subjects' stability skills during free-hand executions.

*experiment #2: evaluate which control approach is more suited to provide the user with intuitive guidance and effective and accurate positioning of the tool on the soft tissues.* Two torque-based impedance assisted modes (GC and SV) are compared to the ADM mode. The *global* and *approaching* performance indexes were compared among N, NS, and ES users. This comparison aimed at showing if the variable dynamic behavior of the robotic assistant in the SV mode can enhance the human-robot cooperation with respect to the state-of-the-art robotic controller during the guidance along wide motions.

*experiment #3: evaluate which control approach is more suited to guarantee a safe contact during tissue's indentation*. The *global* performance indexes computed for the all five different assisted modes (GC, SV, FFE, SVFFE, ADM) were compared among the novices and experts surgeons. This comparison focused on the neurosurgeons participants and investigated if the introduction of an augmented haptic perception on the torque-based impedance approaches (FFE and SVFFE) can limit the unwanted forces applied on the soft tissue (overshooting), thus the risk of penetration.

The neurosurgeons were asked to fill a questionnaire for the qualitative evaluation of the different robotic assisted controllers, defining the preferred cooperative modality during the experiments. After the modulation criteria were explained and further tested on the gelatin phantoms, the neurosurgeons were asked to comment their effectiveness and usability together with the image-based navigation system.

**Table 4.2** Performed experiments.

| | **Objective** | **Users** | | | **Robotic assistance** | | | | | **FH mode** | **Indexes** | | |
|---|---|---|---|---|---|---|---|---|---|---|---|---|---|
| | | **N** | **NS** | **ES** | **GC** | **SV** | **FFE** | **SVFFE** | **ADM** | | **G** | **A** | **H** |
| #1 | *Contact stability* | x | x | x | x | x | x | x | x | x | | | x |
| #2 | *Usability and accuracy* | x | x | x | x | x | | | x | | x | x | |
| #3 | *Tissue indentation Safety* | | x | x | x | x | x | x | x | | x | | |

## 4.2 Results

### 4.2.1 Experiment #1

The amplitude variability indexes ($V_F$ and $V_P$) were computed among trials ($b$ = 1,…,B) and subjects ($u$ = 1,…,U) in each execution modality ($k$ = FH, GC, SV, FFE, SVFFE,

ADM) and in each user group ($g$ = N, NS, ES). A global amplitude variability index, reported in Table 4.3, was computed for each $g$ and $k$ as:

$$V_{Fk,g} = \sqrt{\frac{1}{B \cdot U} \sum_{b=1}^{B} \sum_{u=1}^{U} V_{F\,k,g,b,u}^{\,2}} \quad V_{Pk,g} = \sqrt{\frac{1}{B \cdot U} \sum_{b=1}^{B} \sum_{u=1}^{U} V_{P\,k,g,b,u}^{\,2}} \tag{4.7}$$

For all collected samples, both $V_F$ and $V_P$ indexes in freehand modality ($k$ = FH) results greater than in the robotic assisted cases. During the assisted task executions, the amplitude variability of the measured force (lower than the force measurement accuracy, 0.02N) and penetration level (lower than the measurement accuracy of the optical tracking system, 0.1mm) results reduced by a factor of 10 with respect to the freehand modality (above 0.13N and 1.3mm, respectively). Considering the users' skills during free-hand execution, the hand tremor is more relevant for the naive users with respect to novice and expert neurosurgeons, as shown by a $V_P$ value greater than 2mm. Although comparable $V_P$ values (lower than 1.5mm) are reported between NS and ES surgeons, an higher $V_F$ index for the NS group indicates that the holding equilibrium during the free-hand indentation is found at an higher penetration level with respect to the ES group.

**Table 4.3** Amplitude variability analysis

| $V_P$ [mm] | **Task Execution Modalities** | | | | | |
|---|---|---|---|---|---|---|
| | ***FH*** | ***GC*** | ***SV*** | ***FFE*** | ***SVFFE*** | ***ADM*** |
| **N** | 2.1* | <0.1 | <0.1 | | | <0.1 |
| **NS** | 1.3* | <0.1 | <0.1 | <0.1 | <0.1 | <0.1 |
| **ES** | 1.3* | <0.1 | <0.1 | <0.1 | <0.1 | <0.1 |
| $V_F$ [N] | **Task Execution Modalities** | | | | | |
| | ***FH*** | ***GC*** | ***SV*** | ***FFE*** | ***SVFFE*** | ***ADM*** |
| **N** | 0.21* | <0.02 | <0.02 | | | <0.02 |
| **NS** | 0.21* | <0.02 | <0.02 | <0.02 | <0.02 | <0.02 |
| **ES** | 0.13* | <0.02 | <0.02 | <0.02 | <0.02 | <0.02 |

(*) the assumption ($V_{FH} > V_k$), $k$ = GC,SV,FFE,SVFFE,ADM is verified among trials and users.

### 4.2.2 Experiment #2

Three assisted modalities (GC, SV and ADM) were compared among N, NS and ES using the aforementioned *approaching* and *global* performance indexes (Figure 4.5). For each index, the median value and the first and third IQRs were computed over different trials and different users. A comparative analysis of the different task execution modalities (GC, SV, ADM) and of the different user's groups (N, NS and E) was carried out using the Kruskal-Wallis test with Bonferroni-Holm correction ($p<0.05$) (Holm, 1979).

Figure 4.5a shows that the mean exerted forces ($F_g$) applied with the SV controller (median value below 3.2N) are comparable to the one applied with the GC controller and reduced by 60% with respect to the ADM controller (median value above 5N) for all the groups. Although the forces applied by the generic users during the cooperation in the SV mode are greater than the ones applied by the two neurosurgeons' groups (medians' difference below 1N), the IQRs of the SV populations are reduced by 50% with respect to the other assisted modalities.

As shown in Figure 4.5b, the accelerations (*Acc*) of the SV controller are comparable to those measured with the GC controller (median value greater than $1m/s^2$) and significantly higher (around 50%) with respect to the ADM controller (median value below $0.3mm/s^2$), except for the group E. The IQRs of the GC and ADM populations of the group ES are two times greater than the other groups.

The trajectory smoothness (*S*, Figure 4.5c), computed considering only the last 8cm trajectory towards the target, is comparable among different control modes in all user's group (median value below 0.03), except for the GC trajectories performed by the NS group which result significantly less smooth than the executions in ADM mode and the GC executions performed by the ES group. Accordingly, the execution time index *T* (median value greater than 7s) results 30% greater than the time required in the other assisted modes and for the other user's groups (median values below 5s ), as shown in Figure 4.5d. No significant difference is reported between ADM and torque-based impedance controllers GC and SV.

A lower acceleration zero cross index ($ZC_a$, Figure 4.5e)($p<0.005$) is reported for the ADM mode with respect to GC and SV modes for all users. N presents greater $ZC_a$ index with respect to the neurosurgeons' groups (N, E) for both GC and ADM modes, while no differences are reported among users for the SV mode (median values between 3-5). Although no differences are reported for the neurosurgeons' participants, the GC mode (median start/stop events equal to 8) presents a 50% greater $ZC_a$ index with respect to the SV mode among N.

The global performance indexes are reported in Figure 4.5. The target pointing error ($E_T$, Figure 4.5f) computed among all user's groups and control approaches is comparable to the experimental accuracy of the LWR4+ manipulator reported for repetitive motions (Stein et al. 2009) and respect the clinical accuracy requirement. Although the median pointing accuracy computed with the SV approach for the NS group resulted significantly lower with respect to the ADM approach, it has to be noted that the median values are close to the measurement accuracy threshold (0.3mm).

While significantly greater maximum penetration level ($P_{max}$, Figure 4.5g) and indentation forces ($F_{max}$, Figure 4.5h) are reported for naive users in the ADM mode with respect to the SV and GC modes, no significant difference results between the different control approaches in each neurosurgeons' group. In spite of this, the median values of $F_{max}$ and $P_{max}$ reported for the ES group (median values greater than 0.05N and 9mm respectively) are almost doubled with respect to the NS group, whose median values are close to the relative measurement accuracy thresholds. The contact with the tissue during the task executions performed by NS is not reliably measureable.

As shown from the negative values of the force slope index ($dF$, Figure 4.5i), overshooting during tissue's indentation is significantly present while cooperating in the GC mode with respect to the ADM mode for all user's groups. According to the above mentioned indentation results, the force slope computed in the ADM mode for the novice group is reduced by almost 50% with respect to the other user's groups.

Among naive users, the SV controller combines the positive features of the GC controller, i.e. limited required user's efforts and high reaction capabilities, and of the ADM controller, i.e. reduced force overshooting during tissues contact and intermediate

values of velocity changes ($ZC_a$) along the trajectory. On the other hand, the advantages of the SV controller are not so relevant for the neurosurgeons participants, who encompassed different strategies during the task execution. In particular, the guidance of the novice surgeons resulted conservative within all the assistive modalities, as confirmed by the limited measured forces and penetration level on the tissues. The time required to perform with GC a smooth trajectory with comparable target accuracy is significantly increased with respect to SV mode. Differently, expert neurosurgeons showed more confidence during the target approaching, as confirmed by comparable time executions and smoothness indexes. In this case, a higher target pointing error is reported for the GC mode with respect to the SV mode. Although the torque-based impedance approaches (SV and GC) were shown to significantly improve the usability of the system, i.e. reducing user's efforts with respect to the state-of-the-art admittance controller (ADM), the SV criterion was shown to enhance in a relevant way the human-robot cooperation only for naive users.

### 4.2.3 Experiment #3

All the assisted modalities (GC, SV, FFE, SVFFE and ADM) were compared among the neurosurgeon participants, i.e. the novices and the experts, to evaluate the effectiveness of augmented haptic perception.

The *global* performance indexes are reported in Figure 4.6. No statistically significant differences are reported between control approaches in each user group for the targeting error index ($E_T$, Figure 4.6a), except for an increased pointing accuracy of the FFE mode (target pointing error close to the 0.3mm measurement accuracy threshold and comparable to SVFFE, ADM and GC mode) with respect to the SV mode in the N group. Significant reductions of the penetration level ($P_{max}$ median values below 0.6mm) and of the maximum indentation force ($F_{max}$ median values between 0.03-0.05N) are reported for the ES group when cooperating with FFE and SVFFE, as shown in Figure 4.6b-c. At the same time, the force overshooting ($dF$) in the NS group is significantly reduced (positive median value for both FFE and SVFFE populations), as shown in Figure 4.6d. The FFE criteria was shown to significantly improve the safety level during tissue's indentation performed by neurosurgeons, both novice and experts.

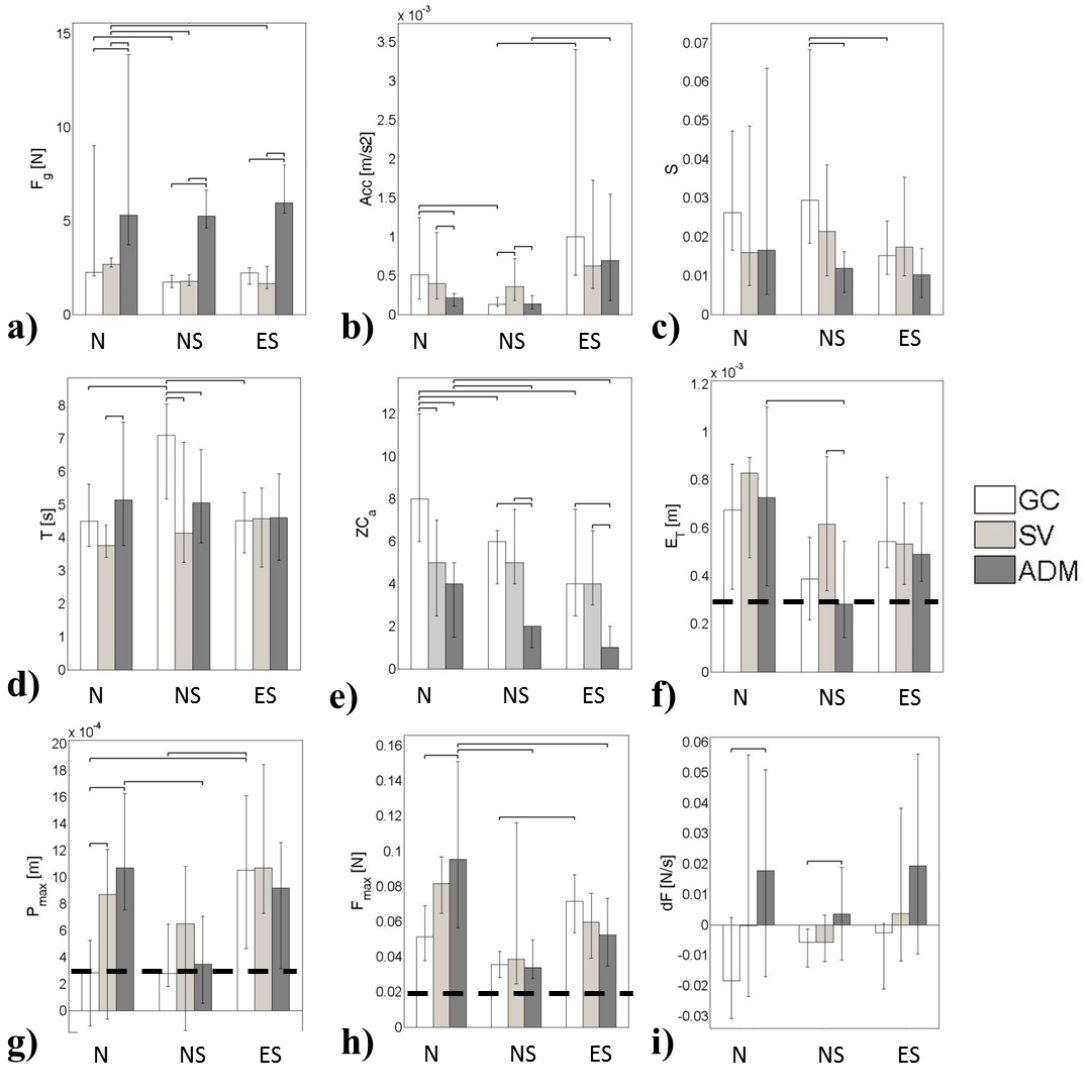


**Figure 4.5** Experimental results of the *approaching* (a-e) and *global* (f-i) performance indexes in comparison #2 between naive users (N), novice surgeons (NS) and expert surgeons (ES) for the three assisted robotic control modes (GC, SV and ADM): a) approaching force ($F_g$); b) maximum norm of the TCP acceleration (*Acc*); c) trajectory smoothness (*S*); d) execution time (*T*); e) acceleration zero crossing index ($ZC_a$); f) target positioning error ($E_T$); g) maximum tissue penetration ($P_{max}$); h) maximum force applied on the tissue ($F_{max}$); i) indentation force slope (*dF*). The accuracy thresholds of the calibrated TCP position measurements (0.3mm) and of the force measurements (0.02N) are also reported.

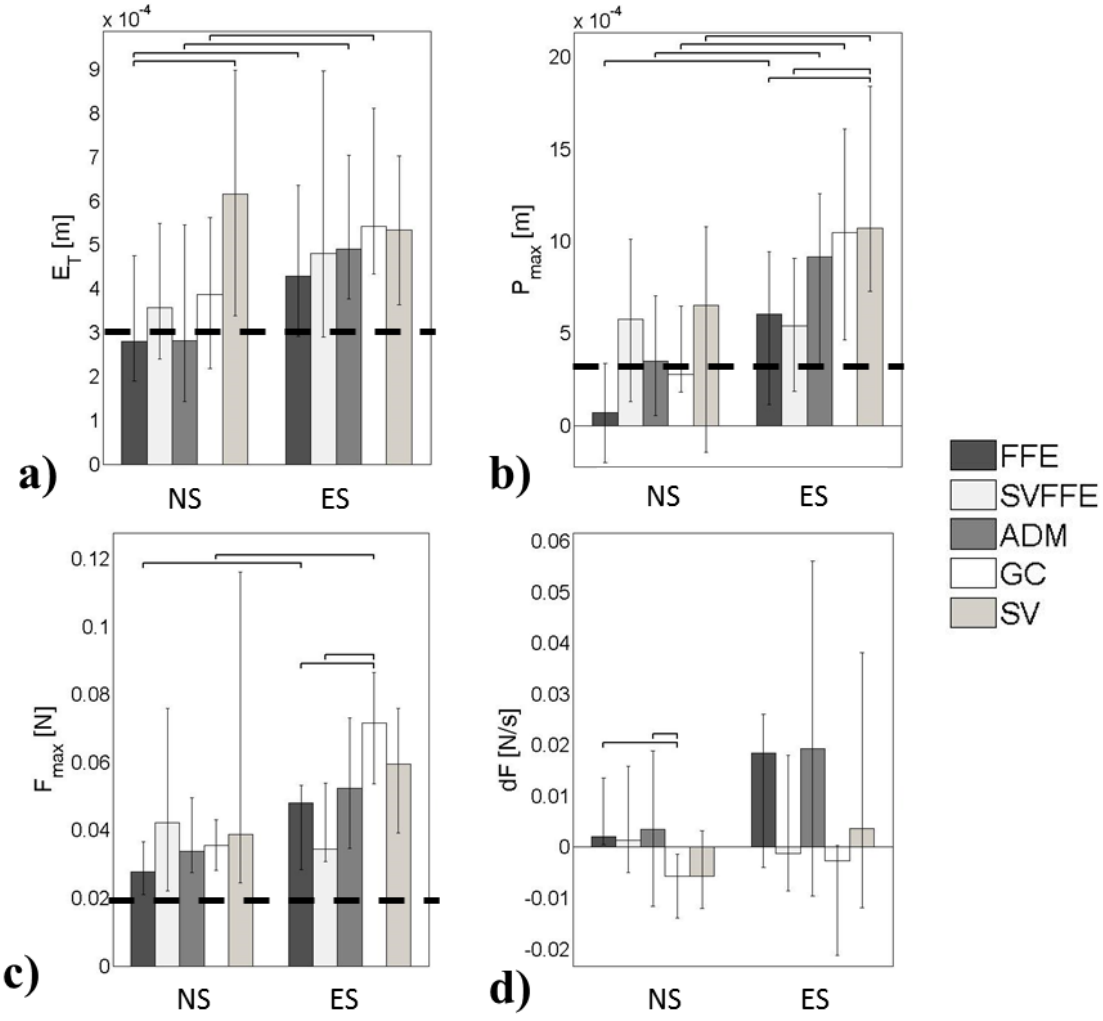


**Figure 4.6** Experimental results of the *global* performance indexes in comparison #3 between novice surgeons (NS) and expert surgeons (ES) for the all five assisted robotic control modes (GC, SV, FFE, SVFFE and ADM): a) target positioning error ($E_T$); b) maximum tissue penetration ($P_{max}$); c) maximum force applied on the tissue ($F_{max}$); d) indentation force slope ($dF$). The accuracy thresholds of the calibrated TCP position measurements (0.3mm) and of the force measurements (0.02N) are also reported.

### 4.2.4 Qualitative assessment

The report of the qualitative assessment of the neurosurgeons are summarized in Table 4.4. The majority of the novice surgeons (3/4) and one expert surgeon (ES2) reported SVFFE as the preferred cooperative modality during the experiments #1, #2, #3, thanks to

the reduced guidance efforts with respect to the ADM mode and the enhanced indentation control on the target with respect to the GC. However, the ADM controller was the preferred cooperative mode for the majority of the expert surgeons (3/4).

**Table 4.4** Qualitative assessment from the enrolled neurosurgeons.

| | **Blind experiments #123** | | **SV**[2] | **FFE**[3] | **General comments** |
|---|---|---|---|---|---|
| | **Preferred modality** | **Relevant difference**[1] | | | |
| **ES1** | SVFFE | SVFFE>GC | + | ++ | ADM is not suitable for required efforts. SVFFE suitable with both hands. SV can be planned preoperatively. |
| **ES2** | ADM | - | + | + | ADM more reliable, the efforts are not tedious. SV should be configured to provide more stiffness at the stimulation target. FFE interesting for subcortical stimulation (under arachnoid) where visual feedback is only partial |
| **ES3** | ADM | - | ++ | / | SV should be configured to provide more stiffness at the stimulation target. FFE not required for cortical stimulation |
| **ES4** | ADM | SVFFE>GC | + | ++ | SV should be configured to provide more stiffness at the stimulation target. FFE interesting even for other applications, providing more confidence during the interaction |
| **NS1** | SVFFE | FFE>GC | + | ++ | ADM is not suitable for required efforts. SV should be configured to provide more stiffness when performing tasks not with the dominant hand |
| **NS2** | SVFFE | FFE>ADM> GC | + | ++ | ADM is not suitable for required efforts. FFE useful to provide more confidence during the interaction |
| **NS3** | SVFFE | SV>GC | ++ | + | ADM is not suitable for required efforts. |
| **NS4** | ADM | - | ++ | / | SV should be configured to provide more stiffness at the target. |

[1] Relevant difference perceived among the torque-based impedance controllers: no difference perceived (-);
[2] Usability of the Space Variable damping criterion: bad (--), indifferent (/), good (+), very good (++);
[3] Usability of the Force Feedback Enhancement criterion: bad (--), indifferent (/), good (+), very good (++).

After the different control modalities were explained and further tested on the gelatin surface with the image-based navigation system, neurosurgeons declared the SV criterion very useful in order to reduce the efforts required to guide the robot from/to the rest configuration, if an higher stiffness could be guaranteed near the stimulation point. Also, the FFE criterion was evaluated (by 6/8 neurosurgeons) as very useful in order to reduce the risk of penetration and provide haptic perception, especially when the stimulation point is covered (under the arachnoid layer) and the visual feedback is only partial (ES2).

## 4.3 Discussion

This work presents the preliminary performance assessment of an enhanced torque-based impedance controller to cooperatively assist the neurosurgeon during targeting tasks in open-skull neurosurgery, such as during intraoperative neurophysiological monitoring (Spena et al. 2013). Differently from high demanding surgical procedures, such as vitreoretinal surgery (Uneri et al. 2010) and/or needle insertion procedures (De Lorenzo, Koseki et al. 2013), force-to-motion control schemas, which provides high accuracy control in a reduced working space (He et al. 2014), may be not the best suited solution for wide motion targeting tasks. The proposed control approach exploits a high compliant dynamic behavior (Albu-Schäffer et al. 2004) combined with two different modulation strategies, which improve the surgeons' ability in performing a safe, stable and accurate contact with the soft tissue. The SV damping criterion (Chapter 2), i.e. modulation of the viscosity parameter of the manipulator along the target approaching trajectory, and the force feedback enhancement criterion (Chapter 3), i.e. non-linear augmentation of the tissue's interaction force, were independently evaluated and combined together in a realistic scenario, mimicking stimulation procedures on soft tissues, with a pool of naive users and neurosurgeons.

To be applied to a redundant manipulator, the Cartesian control approach was defined in the framework of the hierarchical task prioritization (Sentis and Khatib, 2005) and combined with a posture damping strategy to control the position of the robotic elbow

during the assisted cooperation. The modulation criteria were exploited to evaluate only the guidance of the tool tip position, while the tool orientation was maintained fixed implementing rotational virtual fixtures, and the user's handle was positioned close to the end-effector in order to reduce the residual torques applied. The approach presented can be generalized to control the tool orientation, as presented in Paragraph 2.2.3. The potential use of different guidance virtual fixtures, which enable the surgeon to guide the surgical instrument independently along translational or rotational directions, according to his/her actual motion need, during different steps of the surgical workflow is not addressed in this work, but would be subject of investigation in the future.

The robotic assistance (experiment #1) proved to significantly limit the hand tremor and positioning variability (below the absolute measurements accuracy thresholds, respectively 0.02N and 0.1mm) occurring during the free-hand task executions (RMS variability indexes above 0.13N and 1.3mm), also for the naive users who showed a lightly decreased stability skill with respect to the neurosurgeon participants.

Torque-based impedance approaches significantly improve the usability and maneuverability of the system with respect to the state-of-the-art ADM controller (experiment #2), i.e. reducing user's efforts and increasing the reaction capability of the system. In spite of this, the SV criterion allowed enhancing the human-robot cooperation in a relevant way only for the naive users, as shown by an increased confidence during the approaching guidance (decreased $ZC_a$) and reduced overshooting events during tissue's indentation (positive force slopes, $dF$ index) with respect to the constant zero stiffness controller (GC). The neurosurgeons participants encompassed different strategies during the task executions: while the guidance of the novice surgeons was conservative, as confirmed by the limited measured forces and penetration level measured on the tissues, the expert neurosurgeons showed more confidence during the target approaching, guaranteeing the contact with the soft tissue (about 1mm indentation) using visual feedback to detect when indentation occurs. In this context, the SV modality allowed the novices to perform in a reduced execution time (almost 30%) comparable accurate and smooth trajectories and the expert to perform more accurate targeting (almost 20%) task in a comparable execution time.

Although the above-mentioned advantages of the SV controller are not enough to justify the use of this control criterion by itself, its combination with the FFE criterion (experiment #3) allowed a significant reduction of the force overshooting for novices (more than 80%) and of the maximum indentation force for experts (almost 30%), thus significantly improving the safety level during tissue's indentation.

*Qualitative assessment* - Despite the higher efforts required and the comparable indentation performances, the majority of the expert surgeons reported ADM as the preferred cooperative modality, due to the fact that it was perceived as more precise to modulate the forces applied to the tissue at the end of the approaching trajectory. The only expert surgeon without previous experience with automatic or tele-operated robotic systems (ES2), who is acquainted in performing glioma surgery procedures in eloquent areas, declared that the efficiency and maneuverability of the SVFFE controller are highly appreciated with respect to ADM. These features were considered critical factors for the clinical acceptability of the system. Indeed, although requiring for a less compliant behavior of the robot near the target, the majority of the participants (6/8 between novices and experts) evaluated positively the SV criterion in combination with the image-based navigation system, which allowed to easily configure the damping field according to the actual intention of motion. Similarly, the FFE criterion was highly appreciated by the majority of the participants (6/8 between novices and experts), once tested in unconstrained targeting tasks on the gelatin phantoms. During the experimental session, the surgeons were required to perform the tool placement with as less tissue's indentation as possible. Thus, the unaware users did not fully exploits the potentiality of the FFE approach and mostly relied on visual feedback only. However, a significant reduction in the risk of tissue's penetration was quantified among novices and experts. It is to be noted that the same FFE approach was combined also with the ADM controller, but in that case no haptic perception was provided to the user because the augmented tissue's force were applied on top of greater motion guidance forces, thus the force sensitivity was highly reduced.

The use of an human-machine interface for the online configuration of the damping fields of the SV criterion, according to the user's intention of motions, was proved feasible in the

brain cortex stimulation scenario. It has to be noted that the brain-mimicking gelatin phantoms were modelled as static objects in the image-based navigation system and registered one time to the experimental scene. Conversely, this coherence between patient-specific images and the intraoperative reality is not guaranteed during open-skull craniotomy because of brain shift (Miga et al. 1999), which was measured almost 17mm after 94 minutes after the dura opening (Roberts et al. 1998). The brain displacement occurring between repetitive stimulation on the same site (10-15 minutes maximum elapsed time) can be considered negligible, thus is expected not to affect the repetitive cooperative guidance based on the previously acquired target point. Nevertheless, this issue can affect the possibility of providing graphical image-based stimulation maps of the whole procedure, which can overcome the use of sterile tags with numbers or letters placed on stimulation-sensitive spots, currently used for visualizing the cortical areas involved in motor, cognitive or language functions (Duffau, 2010). For this purpose, the image-based navigation system can potentially be combined with approaches for the real time compensation of the brain shift, e.g. intraoperative imaging systems (Nabavi et al. 2001) (Blumenthal et al. 2005) or brain deformation models (Wittek et al. 2005) together with intra-operative stereo vision systems (Faria et al. 2014) for the runtime tracking of brain anatomical features.

The main limitation of the study is that the viscosity level provided by the SV criterion on target was set in order to mimic the human arm damping effect (as defined in Paragraph 2.2.4), without a parameter tuning based on the neurosurgeon's skills. In fact, the robot's stiffness on the stimulation point was perceived as insufficient by the surgeons who felt insecure in pointing and maintaining the position on the target. However, the upper boundaries of the SV modulation (30Ns/m) can be further increased to reach the constant damping value (300Ns/m) set for the constant admittance control, which was considered adequate by the expert surgeons. One of the expert neurosurgeons also pointed out that the high compliant behavior of the manipulator far away from the surgical area, which made the assistant intuitive and easy to be used during the wide motion from/to the rest configuration, can be critical if unwanted interaction occurs. This weakness of the system can be overcome combining the proposed modulation criteria, which focused on

guaranteeing a safe contact with the soft tissue, with a velocity-based variable impedance criterion (Erden and Marić, 2011), which can be used to increase the stiffness of the manipulator when no interaction is detected, thus its ability in reject disturbances.

In conclusion, the SVFFE controller showed comparable performances with respect to the state-of-the-art constant admittance schema, allowing for an accurate, i.e. the target pointing accuracy (below 1mm) respects the clinical requirement, stable, i.e. reduction of the free-hand tremor by a factor of 10 during the holding phase, and safe, i.e. 80% reduction of the indentation overshooting, contact with the soft tissues, but, in addition, it provides a significant reduction of the user efforts and a greater maneuverability during wide motion guidance. The use of an image-based navigation system to intra-operatively configure the SV damping field is appreciated, although the expert neurosurgeons underlined the necessity of tuning differently the dynamic parameters of the SV modulation, in order to increase the reliability of the system, currently perceived not sufficient. Future work will address the combination of the SVFF approach with velocity-based impedance modulation criteria in order to ensure safety interaction with the manipulator in the operating theatre when no tissue contact is performed.

# Chapter 5

# Conclusions

This PhD thesis investigated the possibility of introducing a cooperative-control robotic device to efficiently assist the surgeon during specific tasks in open-skull neurosurgery, which are currently performed free-hand. The traditional surgical approach can benefit from robotic assistance during the execution of brain targeting task, where the surgical instrument needs to be maintained in arbitrary stable position with high accuracy, thus increasing the clinical outcomes of the procedures and/or reducing the neurosurgeon's execution efforts. A particular procedure is addressed, which is exemplary in terms of requirements (1mm pointing accuracy, 0.03-0.3N indentation contact forces): brain cortex stimulation. During stimulation, the neurosurgeon repeatedly performs free-hand accurate placements of the stimulator and holds it on delicate soft tissues. Such gesture can be affected by hand tremor and reduced haptic perception. With an hands-on robotic assistant in the operating room, the stimulation sites can be performed in a more accurate way, as shown in Chapter 2 and Chapter 4, where we demonstrated that the hand tremor of neurosurgeons during free-hand execution (above 1mm) can be reduced by 2 orders of magnitude guaranteeing the respect of the clinical accuracy requirements. At the same time, the robotic device can aid the surgeon guaranteeing tissue's contact safety, as discussed in Chapter 3 and Chapter 4, where we proved that augmented haptic perception reduces the tool-tissue interaction forces during indentation, thus potentially avoiding the risk of penetration during unwanted motions.

This work represents a small but significant step forward in the design of cooperative-controlled robotic devices and in the study of their applicability for novel surgical procedures, both from a scientific and clinical point of view, thanks to the close collaboration with researchers at the Imperial College, London (UK), and a pool of novice and expert neurosurgeons coming from different institutions, such as "Ospedale Pedriatrico

Bambin Gesù" (Rome, Italy), "Istituto Clinico Carlo Besta" (Milan, Italy) and "Ospedale Niguarda" (Milan, Italy).

The PhD work contributed to:

*(i) investigate the best control strategy for a comfortable and effective cooperation during the targeting approaching.*

Robotic assisted targeting tasks in open-skull surgery, such as during brain cortex stimulation, require millimeter position accuracy to precisely place the instrument on the target of interest and are usually repeated multiple times in different workflow steps during the surgical procedure (Paragraph 1.2.1). In Chapter 2, an enhanced torque-based impedance controller is specifically designed to improve the human-robot cooperation along the repetitive wide guidance trajectories from/to resting configuration, exploiting the "soft" dynamic behavior of a lightweight robot, for which the standard force-to-motion control schema proposed in literature (Uneri et al. 2010)(De Lorenzo, Koseki et al. 2013) would be less suitable (Lawrence, 1998). The potentiality of different variable impedance criteria is well-known in the literature and already applied in surgical (Kazanzides et al. 1992), industrial (Duchaine et al. 2012) and robotic assistive (Nishiwaki and Yano, 2008) applications. The novel variable damping controller (Paragraph 2.2.3), based on the knowledge of the surgeon's intention of motion, was proved to combine the positive features of two well-known impedance controllers with fixed dynamic parameters, identified as the most transparent and the optimal constant damping controllers, coupled with the smooth and intuitive convergence to the target. It was shown that the reaching task under laboratory condition result in reduced targeting error, which guarantees the respect of the position accuracy requirement, and user efforts, which ensure that assisted tool trajectories feel natural to the user (Paragraph 2.4).

*(ii) investigate the best control strategy for a safe and stable placement of the surgical instrument on the soft tissue during the tool placement.*

The contact between the surgical instrument and the underneath soft tissue must be guaranteed stable, filtering hand tremors (MacLachlan et al. 2012), and safe, preventing any damage to the tissue due to indentation (Paragraph 1.2.1). The haptic perception provided by the proposed non-linear force feedback controller (Paragraph 3.2.1) is shown to improve

the user's skill in performing tool's placement on brain-mimicking soft tissue, both in terms of contact stability, i.e. reduction of the free-hand tremor by a factor of 10, and contact safety, i.e. 50% reduction of the indentation level, as discussed in Chapter 3. Although it does not provide perception of the mechanical characteristics of the tissue as the linear approaches (De Lorenzo, Koseki et al. 2013), the use of non-linear modulation allows the augmentation of the small forces during the first phase of tissue's indention and gives the user the perception of a soft "virtual" barrier, which indicates that the contact has occurred. At the same time, the possibility of consciously penetrating the tissue is guaranteed to the surgeon by a saturation level on the force feedback. In this work, the parameters of the FFE controller were optimally tuned based on the mechanical characteristics of the brain-mimicking phantoms, and set constant during the contact. In order to generalize the approach to softer/harder tissues, adaptive criteria based on the online estimate of the environmental stiffness (Tsumugiwa et al. 2002) or on active stability observers (Duchaine et al. 2012) should be added to the FFE controller.

*(iii) preliminary study the feasibility of the proposed impedance control approaches with a pool of expert neurosurgeons for its application to brain cortex stimulation procedures.*

The performance validation of the two modulation criteria based on the torque-based impedance control approach was performed by naïve users and neurosurgeons on a realistic setup for brain cortex stimulation using brain-mimicking phantoms, as described in Chapter 4. The combination of the proposed criteria (SVFFE controller) showed comparable performances with respect to the state-of-the-art constant admittance schema (Lawrence, 1998), allowing for the accurate, i.e. the target pointing accuracy (below 1mm) respects the clinical requirement, stable, i.e. reduction of the free-hand tremor by a factor of 10 during the holding phase, and safe, i.e. 80% reduction of the indentation overshooting, contact with the soft tissues, but providing, in addiction, a reduction of the user efforts and a greater maneuverability of the system. Although the expert neurosurgeons underlined the necessity to differently tune the dynamic parameters of the SV criterion (Paragraph 4.3), in order to increase the perceived reliability of the system in performing precise targeting tasks, the use of an image-based navigation system to intra-operatively configure the damping field is

proved feasible for brain cortex stimulation procedure. The preliminary study underlined the necessity to include in the control system additional modulation criteria of the robot dynamics, such as velocity-based variable impedance criteria (Erden and Marić, 2011), to increase the safety of the procedure also when the manipulator is in a resting configuration far away from the surgical area, in case of unintentional interactions. Tests on this issues are already on going at NearLab.

The results presented in this work supported the feasibility of the use of an hands-on controlled manipulator during brain cortex stimulation procedures, for which new methodologies for intuitive human-robot and safe robot-tissue interaction control were specifically designed and validated. The proposed control system might a starting point for the future development of assistive devices in open-skull neurosurgery, for which the current CAS methods may not be suitable (Barbosa et al. 2014), thus increasing the safety of the conventional procedures. The use of cooperatively controlled manipulator to assist brain cortex stimulation procedures might have a significant impact on the clinical reliability of the intraoperative monitoring technique. Indeed, active constraints control (Bowyer et al. 2013) might be exploited to guide the surgeon towards previously recorded sites in order to perform repetitive stimulation with high accuracy. Moreover, technologies for the real-time compensation of the brain shift (Miga et al. 1999), e.g. intraoperative imaging systems (Nabavi et al. 2001) (Blumenthal et al. 2005) or brain deformation models (Wittek et al. 2005) together with intra-operative stereo vision systems (Faria et al. 2014), may be combined with the image-based navigation system we proposed. Hence, the intraoperative functional map of the stimulation can potentially be provided, avoiding the use of tags labelling on the cortex.

This work is in line with the actual research trend in medical robotics, which propose devices that are *effective, safe,* both for the patient and the clinical staff in the OR, and at the same time that provide the surgeon with interfaces as *intuitive* and *familiar* as possible, in order to reduce the training period and facilitate the acceptance of the technology in clinics. Cooperatively controlled surgical manipulators (De Lorenzo, Koseki et al. 2013)(Uneri et al. 2010)(Pearle et al. 2009) have been proposed to meet these needs in

different surgical scenarios, also supported by methods and technologies developed to improve the human-robot cooperation in industrial robotics (Erden and Marić, 2011) and assistive robotics (Duchaine et al. 2012) (Nishiwaki and Yano, 2008).

One collateral aspect of this research, that we consider particularly interesting, is the implicit confirmation that redundant manipulator might introduce relevant advantages with respect to 6 DoFs robotic system, despite of the higher cost of the system. Even if it was not investigated directly in this work, we want to point out that the enrolled surgeons with previous experience with cooperative-controlled manipulation systems (Lefranc et al. 2014) (Hughes et al. 2013) highly appreciated the increased manoeuvrability introduced by the $7^{th}$ DoF of the system proposed. Future work needs to be address to determine the optimal control strategy to manage the robot's redundancy, in particular the more suited to minimize the encumbrance in the operating room while guaranteeing high maneuverability at the end-effector. Tests on this issues are already on-going.

From another prospective, this work discuss the potentialities of an adapted industrial manipulator for human-robot cooperation in a clinical scenario. Indeed, the research interest in "soft robotics", aimed at making the robots able to "interact with unknown environments and cooperate in a safe manner with humans, while approaching their performances in terms of weight, force and velocity" (Albu-Schäffer et al. 2011), has been increasing in the last decades. During cooperation, humans should feel assured that they understand the robot's intentions and the robot must execute its tasks with motion profiles that humans perceive as natural (Zanchettin et al. 2013). The results reported in this work underlined some critical aspects of the LWR4+ manipulator in terms of transparency features and can be useful material for improving the next generations of lightweight robots.

The experiments we developed in this work were preliminary, used to prove a concept, but future research based on our results will show to what extend can a cooperative manipulator improve surgeon's skills during open-skull procedures.

# Bibliography


Abolhassani N, Rajni P, Mehrdad M. 2007. Needle insertion into soft tissue: A survey. Medical Engineering & Physics. 29(4): 413-431.

Albu-Schäffer A, Ott C, Hirzinger G. 2004. A passivity based cartesian impedance controller for flexible joint robots - part ii: fullstate feedback, impedance design and experiments. In Proc. of IEEE Int. Conf. on Robotics and Automation. 3: 2666–2672.

Albu-Schäffer A, Eiberger O, Fuchs M, Grebenstein M, Haddadin S, Ott C, Stemmer A, Wimbock T, Wolf S, Borst C, Hirzinger G. 2011. Anthropomorphic soft robotics–from torque control to variable intrinsic compliance. In: Robotics Research. Springer Berlin Heidelberg; p. 185-207.

Barbosa BJAP, Mariano ED, Batista CM, Marie SKN, Teixeira MJ, Pereira CU, Tatagiba MS, Lepski GA. 2014. Intraoperative assistive technologies and extent of resection in glioma surgery: a systematic review of prospective controlled studies. NEUROSURG REV. p. 1-11.

Beez T, Boge K, Wager M, Whittle I, Fontaine D, Spena G, Braun S, Szelènyi A, Bello L, Duffau H, Sabel M. 2013. Tolerance of awake surgery for glioma: a prospective European Low Grade Glioma Network multicenter study. Acta neurochirurgica. 155(7): 1301-1308.

Berkelman PJ, Whitcomb LL, Taylor RH, Jensen P. 2000. A miniature instrument tip force sensor for robot/human cooperative microsurgical manipulation with enhanced force feedback. In: Medical Image Computing and Computer-Assisted Intervention–MICCAI 2000. Springer Berlin Heidelberg; p. 897-906.

Besl PJ, Mckay ND. 1992. Method for registration of 3-D shapes. In: Robotics-DL tentative. International Society for Optics and Photonics; p. 586-606.

Bizzi E, Hogan N, Mussa-Ivaldi FA, Giszter S. 1992. Does the nervous system use equilibrium-point control to guide single and multiple joint movements. Behav Brain Sci. 15: 603-613.

Blumenthal T, Hartov A, Lunn K, Kennedy FE, Roberts DW. Paulsen KD. 2005. Quantifying brain shift during neurosurgery using spatially tracked ultrasound. In: Proceedings of SPIE Medical Imaging 2005; p. 388-399.

Bowyer SA, Davies BL, Rodriguez y Baena F. 2013. Active Constraints/Virtual Fixtures: A Survey. IEEE TRANSACTIONS ON ROBOTICS. 30(1): 138-157.

Burdet E, Osu R, Franklin DW, Milner TE, Kawato M. 2001. The central nervous system stabilizes unstable dynamics by learning optimal impedance. Nature. 414: 446–449.

Cardinale F, Cossu M, Castana L, Casaceli G, Tassi L, Francione S, Nobili L, Gozzo F, Proserpio P, Lo Russo G. 2013. Five Hundred Stereoelectroencephalography Procedures For Presurgical Invasive Evaluation Of Drug-resistant Epilepsy: Efficiency, Safety, Application Accuracy And Outcome On Seizures, 15. In: Stereotactic and functional neurosurgery 91 (Suppl 1).

Comparetti MD, De Momi E, Beyl T, Kunze M, Raczkowsky J,Ferrigno G. 2014. Convergence Analysis of an Iterative Targeting Method for Keyhole Robotic Surgery. International Journal of Advanced Robotic Systems. 11(60): 1-8.

Dalvand MM, Shirinzadeh B, Nahavandi S, Smith J. 2014. Effects of realistic force feedback in a robotic assisted minimally invasive surgery system. Mim Invasiv Ther. 23(3): 127-135.

Dashti R, Rinne J, Hernesniemi J, Niemelä M, Kivipelto L, Lehecka M, Karatas A, Avci E, Ishii K, Shen H, Pelàez JG, Albayrak BS, Ronkainen A, Koivisto T, Jääskeläinen JE. 2007. Microneurosurgical management of proximal middle cerebral artery aneurysms. Surgical neurology. 67(1): 6-14.

Davies B. 2000. A review of robotics in surgery. Proc Inst Mech Eng H. 214(1):129-40.

Davies B, Harris SJ, Rodriguez y Baena F, Gomes P, Jakopec M. 2004. Hands-on robotic surgery: is this the future? In: Medical Imaging and Augmented Reality. Springer Berlin Heidelberg; p. 27-37.

Davies B, Jakopec M, Harris SJ, Rodriguez y Baena F, Barrett A, Evangelidis A, Gomes P, Henckel J, Cobb J. 2006. Active-constraint robotics for surgery. Proceeding of the IEEE. 94(9):1696-1704.

Davies BL, Rodriguez y Baena F, Barrett ARW, Gomes MPSF, Harris SJ, Jakopec M, Cobb JP. 2007. Robotic control in knee joint replacement surgery. Proceedings of the Institution of Mechanical Engineers, Part H: Journal of Engineering in Medicine. 221(1): 71-80.

De Lorenzo D, Koseki Y, De Momi E, Chinzei K, Okamura A. 2011. Experimental evaluation of a coaxial needle insertion assistant with enhanced force feedback. In: Proceedings of 33rd Annual international Conference of the IEEE Engineering in Medicine and Biology Society 2011; p. 3447-3450.

De Lorenzo D, Koseki Y, De Momi E, Chinzei K, Okamura AM. 2013. Coaxial Needle Insertion Assistant With Enhanced Force Feedback. IEEE T Bio-Med Eng. 60(2): 379-389.

De Lorenzo D, De Momi E, Conti L, Votta E, Riva M, Fava E, Bello L, Ferrigno G. 2013. Intraoperative forces and moments analysis on patient head clamp during awake brain surgery. Medical & Biological Engineering & Computing. 51(3): 331-341.

Demi B, Ortmaier T, Seibold U. 2005. The touch and feel in minimally invasive surgery. In: Proc. IEEE Int. Workshop Haptic Audio Visual Environ. Appl. 2005; p. 33-38.

Dogangil G, Davies BL, Rodriguez y Baena F. 2010. A review of medical robotics for minimally invasive soft tissue surgery. Proceedings of the Institution of Mechanical Engineers, Part H: Journal of Engineering in Medicine. 224(5): 653-679.

Duchaine V, Gosselin CM. 2007. General Model of Human-Robot Cooperation Using a Novel Velocity Based Variable Impedance Control. In: Proc.World Haptics Conf, 2007; p. 446-451.

Duchaine V, Gosselin CM. 2008. Investigation of human-robot interaction stability using Lyapunov theory. In: Proc. of IEEE Int. Conf. on Robotics and Automation 2008; p. 2189-2194.

Duchaine V, St-Onge BM, Gao D, Gosselin C. 2012. Stable and Intuitive Control of an Intelligent Assist Device. IEEE Trans Haptics. 5(2): 148-159.

Duffau H. 2010. Brain mapping in neuro-oncology: what is the future?. Future Neurology. 5(3): 433-448.

Dziedzic T, Bernstein M. 2014. Awake craniotomy for brain tumor: indications, technique and benefits. Expert review of neurotherapeutics. p. 1-11.

Engh JA, Minhas DS, Kondziolka D, Riviere CN. 2010. Percutaneous intracerebral navigation by duty-cycled spinning of flexible bevel-tipped needles. Neurosurgery. 67(4): 1117-1123.

Erden MS, Marić B. 2011. Assisting manual welding with robot. Robot Cim-Int Manuf. 27(4): 818-828.

Faria C, Sadowsky O, Bicho E, Ferrigno G, Joskowicz L, Shoham M, Vivanti R, De Momi E. 2014. Validation of a stereo camera system to quantify brain deformation due to breathing and pulsatility. Medical physics. 41(11): 113502.

Fedorov A, Beichel R, Kalpathy-Cramer J, Finet J, Fillion-Robin JC, Pujol S, Bauer C, Jennings D, Fennessy F, Sonka M, Buatti J, Aylward SR, Miller JV, Pieper S, Kikinis R. 2012. 3D Slicer as an Image Computing Platform for the Quantitative Imaging Network. Magn Reson Imaging. 30(9):1323-41.

Ferrand-Sorbets S, Taussig D, Fohlen M, Bulteau C, Dorfmuller G, Delalande O. 2010. Frameless stereotactic robot-guided placement of depth electrodes for stereo-electroencephalography in the presurgical evaluation of children with drug-resistant focal epilepsy. In: CNS Annual Meeting, 2010.

Fitzpatrick JM, West JB. 2001. The Distribution of Target Registration Error in Rigid-Body Point-Based Registration. IEEE T Med Imaging. 20(9): 917-927.

Frasson L, Ko SY, Turner A, Parittotokkaporn T, Davies BL, Vincent JF, Rodriguez y Baena F. 2010. STING: a soft-tissue intervention and neurosurgical guide to access deep brain lesions through curved trajectories. Proceedings of the IMechE, Part H, Journal of Engineering in Medicine. 224(6):775-788.

Frey D, Schilt S, Strack V, Zdunczyk A, Rösler J, Niraula B, Vajkoczy P, Picht T. 2014. Navigated transcranial magnetic stimulation improves the treatment outcome in patients with brain tumors in motor eloquent locations. Neuro-oncology. nou110.

Ganesh G, Albu-Schäffer A, Haruno M, Kawato M, Burdet E. 2010. Biomimetic motor behavior for simultaneous adaptation of force, impedance and trajectory in interaction tasks. In: Proc. of IEEE Int. Conf. on Robotics and Automation, 2010; p. 2705-2711.

Ganesh G, Jarasse N, Haddadin S, Albu-Schaeffer A, Burdet E. 2012. A versatile biomimetic controller for contact tooling and tactile exploration. In: Proc. of IEEE Int. Conf. on Robotics and Automation, 2012; p. 3329-3334.

Gralla J, Nimsky C, Buchfelder M, Fahlbusch R, Ganslandt O. 2003. Frameless stereotactic brain biopsy procedures using the Stealth Station: indications, accuracy and results. Zentralblatt für Neurochirurgie. 64(4): 166-170.

He X, Marcin B, Gehlbach P, Handa J, Taylor R, Iordachita I. 2013. A novel dual force sensing instrument with cooperative robotic assistant for vitreoretinal surgery. In: Proc. of IEEE Int. Conf. on Robotics and Automation, 2013; p. 213-218.

He X, Balicki M, Gehlbach P, Handa J, Taylor RH, Iordachita I. 2014. A Multi-Function Force Sensing Instrument with Variable Admittance Robot Control for Retinal Microsurgery. In: Proc. of IEEE Int. Conf. on Robotics and Automation, 2014; p. 1411-1418.

Holm S. 1979. A simple sequentially rejective multiple test procedure. SCAND J STAT. p. 65–70.

Horn BK. 1987. Closed-form solution of absolute orientation using unit quaternions. JOSA A. 4(4): 629-642.

Hughes G, Vadera S, Bulacio J, Gonzalez-Martinez J. 2013. Robotic placement of intracranial depth electrodes for long-term monitoring: Utility and efficacy. ASSFN Biennial Meeting, 2013.

Ikeura R, Inooka H. 1995. Variable impedance control of a robot for cooperation with a human. In: Proc. of IEEE Int. Conf. on Robotics and Automation, 1995; p. 3097–3102.

Ikeura R, Mizutani K. 1998. Control of Robot Cooperating with Human Motion. In: Proc of IEEE Int Workshop on Robot and Human Communication, 1998; p.525-529.

Ikeura R, Moriguchi T, Mizutani K. 2002. Optimal variable impedance control for a robot and its application to lifting an object with a human. In: Proc of IEEE Int Symp on Robot and Human Interactive Communication, 2002; p. 500–505.

Izumo T, Matsuo T, Morofuji Y, Hiu T, Horie N, Hayashi K, Nagata I. 2014. Microsurgical Clipping for Recurrent Aneurysms After Initial Endovascular Coil Embolization. World neurosurgery.

Jakopec M, Harris SJ, Rodriguez y Baena F, Gomes P, Cobb J, Davies BL. 2001. The first clinical application of a “hands-on” robotic knee surgery system. Computer Aided Surgery. 6(6): 329-339.

Janabi-Sharifi F, Hayward V, Chen CSJ. 2000. Discrete-time adaptive windowing for velocity estimation. IEEE Trans. Control Syst. Technol. 8(6): 1003-1009.

Jarrassé N, Paik J, Pasqui V, Morel G. 2008. How can human motion prediction increase transparency?. In: Proc. of IEEE Int. Conf. on Robotics and Automation, 2008; p. 2134-2139.

Kadiallah A, Franklin DW, Burdet E. 2012. Generalization in adaptation to stable and unstable dynamics. PLoS one. 7(10), e45075.

Karam SD, Tai A, Snider JW, Bhatia S, Bedrick EJ, Rashid A, Jay A, Kalhorm C, Nair N, Harter KW, Collins SP, Jean W. 2014. Refractory trigeminal neuralgia treatment outcomes following CyberKnife radiosurgery. Radiation Oncology. 9(1): 257.

Kazanzides P, Zuhars J, Mittelstadt B, Taylor RH. 1992. Force sensing and control for a surgical robot. In Proc. of IEEE Int. Conf. on Robotics and Automation, 1992; p. 612-617.

Kronander K, Billard A. 2013. Learning Compliant Manipulation through Kinesthetic and Tactile Human-Robot Interaction. IEEE Trans Haptics. 7(3): 367 – 380.

Kubus D, Kroger T, Wahl FM. 2007. On-line rigid object recognition and pose estimation based on inertial parameters. In: Proc. Of the IEEE Int Conf on Intelligent Robots and Systems, 2007; p. 1402–1408.

Kuo JS, Yu C, Petrovich Z, Apuzzo ML. 2003. The CyberKnife stereotactic radiosurgery system: description, installation, and an initial evaluation of use and functionality. Neurosurgery. 53(5): 1235-1239.

Lawrence DA. 1988. Impedance Control stability properties in common implementation. In: Proc. of IEEE Int. Conf. on Robotics and Automation, 1988; p. 1185-1190.

Lefranc M, Capel C, Pruvot AS, Fichten A, Desenclos C, Toussaint P, Le Gars D, Peltier J. 2014. The Impact of the Reference Imaging Modality, Registration Method and Intraoperative Flat-Panel Computed Tomography on the Accuracy of the ROSA® Stereotactic Robot. Stereotactic and functional neurosurgery. 92(4):242-250.

MacLachlan RA, Becker BC, Tabares JC, Podnar GW, Lobes LA, Riviere CN. 2012. Micron: An actively stabilized handheld tool for microsurgery. IEEE Transactions on Robotics. 28(1):195-212.

Marayong P, Hager GD, Okamura AM. 2006. Effect of hand dynamics on virtual fixtures for compliant human-machine interfaces. In: Proc of Int Symp on Haptic Interfaces for Virtual Environments and Teleoperator Systems, 2006; p. 109–115.

Marcus HJ, Zareinia K, Gan LS, Yang FW, Lama S, Yang GZ, Sutherland GR. 2014. Forces exerted during microneurosurgery: a cadaver study. The International Journal of Medical Robotics and Computer Assisted Surgery. 10(2): 251-256.

Maurin B, Barbe L, Bayle B, Zanne P, Gangloff J, De Mathelin M, Gangi A, Soler L, Forgione A. 2004. In vivo study of forces during needle insertions. In Perspective in Image-guided Surgery: Proceedings of the Scientific Workshop on Medical Robotics, Navigation, and Visualization 2004; p. 415-422.

Mayer H, Nagy I, Knoll A, Braun E, Bauernschmitt R, Lange R. 2007. Haptic feedback in a telepresence system for endoscopic heart surgery. MIT Presence, Teleoperators and Virtual Environments. 16(5): 459–470.

Miga MI, Paulsen KD, Lemery JM, Eisner SD, Hartov A, Kennedy FE, Roberts DW. 1999. Model-Updated Image Guidance: Initial Clinical Experiences with Gravity-Induced Brain Deformation. IEEE Trans Med Imaging. 18(10): 866-74.

Miller K, Kiyoyuki C, Girma O, Piotr B. 2000. Mechanical properties of brain tissue in-vivo: experiment and computer simulation. J BIOMECH. 33(11): 1369-1376.

Nabavi A, Black PM, Gering DT, Westin CF, Mehta V, Pergolizzi Jr RS, Ferrant M, Warfield S, Hata N, Schwartz RB, Wells WM, Kikinis R, Jolesz FA. 2001. Serial intraoperative magnetic resonance imaging of brain shift. Neurosurgery. 48(4): 787-798.

Nakamura N, Sugano N, Nishii T, Kakimoto A, Miki H. 2010. A comparison between robotic-assisted and manual implantation of cementless total hip arthroplasty. Clinical Orthopaedics and Related Research. 468(4): 1072-1081.

Nishiwaki K, Yano K. 2008. Variable impedance control of meal assistance robot using potential method. In Proc. of IEEE Int. Conf. on intelligent robots and systems, 2008; p. 3242–3247.

Okamura AM. 2004. Methods for haptic feedback in teleoperated robot assisted surgery. Industrial Robot: An International Journal. 31(6): 499–508.

Okamura AM. 2009. Haptic feedback in robot-assisted minimally invasive surgery. Curr Opin Urol. 19(1): 102–107.

Parittotokkaporn T, Frasson L, Schneider A, Huq SE, Davies BL, Degenaar P, Biesenack J, Rodriguez y Baena FM. 2008. Soft tissue traversal with zero net force: feasibility study of a biologically inspired design based on reciprocal motion. In Proc of the IEE Int Conf on Robotics and Biomimetics, 2008; p. 80-85.

Pearle AD, Kendoff D, Stueber V, Musahl V, Repicci JA. 2009. Perioperative management of unicompartmental knee arthroplasty using the MAKO robotic arm system (MAKOplasty). Am J Orthop. 38(2): 16-19.

Philippsen R, Sentis L, Khatib O. 2011. An Open Source Extensible Software Package to Create Whole-Body Compliant Skills in Personal Mobile Manipulators. In: Proc. of IEEE Int. Conf. on Intelligent Robots and Systems, 2011; p. 1036-1041.

Ritter RC, Quate EG, Gillies GT, Grady MS, Howard MA, Broaddus WC. 1998. Measurement of friction on straight catheters in in vitro brain and phantom material. IEEE T BIO-MED ENG. 45(4):476-485.

Roberts DW, Hartov A, Kennedy FE, Miga MI, Paulsen KD. 1998. Intraoperative brain shift and deformation: a quantitative analysis of cortical displacement in 28 cases. Neurosurgery. 43(4): 749-758.

Roveda L, Vicentini F, Molinari Tosatti L. 2013. Deformation-Tracking Impedance Control in Interaction with Uncertain Environments. In: Proc. of Int Conf on Intelligent Robots and Systems, 2013; p. 1992-1997.

Safwat B, Su EL, Gassert R, Teo CL, Burdet E. 2009. The role of posture, magnification, and grip force on microscopic accuracy. Annals of biomedical engineering. 37(5): 997-1006.

Sanai N, Berger MS. 2010. Intraoperative stimulation techniques for functional pathway preservation and glioma resection. Neurosurgical focus. 28(2), E1.

Sandoval R, MacLachlan RA, Oh M, Riviere CN. 2007. Positioning Accuracy of Neurosurgeons. In: Proc IEEE Eng Med Biol Soc.007; p. 206-9.

Sentis L, Khatib O. 2005. Synthesis of whole-body behaviors through hierarchical control of behavioral primitives. Int J Hum Robot. 2(4): 505–518.

Singer SM, Akin DL. 2011. A Survey of Quantitative Team Performance Metrics for Human-Robot Collaboration. In Proc of Int Conf on Environmental Systems, 2011; 5248(AIAA).

Spena G, Garbossa D, Panciani PP, Griva F, Fontanella MM. 2013. Purely subcortical tumors in eloquent areas: Awake surgery and cortical and subcortical electrical stimulation (CSES) ensure safe and effective surgery. CLIN NEUROL NEUROSUR. 115(9):1595-1601.

Stein D, Monnich H, Raczkowsky J, Worn H. 2009. Visual servoing with an optical tracking system and a lightweight robot for laser osteotomy. In Proc. of IEEE Int. Conf. on Control and Automation, 2009; p. 1896–1900.

Sutherland GR, Latour I, Greer AD. 2008. Integrating an image-guided robot with intraoperative MRI. Engineering in Medicine and Biology Magazine, IEEE. 27(3): 59-65.

Sutherland GR, Wolfsberger S, Lama S, Zarei-nia K. 2013. The evolution of neuroArm. Neurosurgery. 72: A27-A32.

Szelènyi A, Bello L, Duffau H, Fava E, Feigl GC, Galanda M, Neuloh G, Signorelli F, Sala F, Workgroup for Intraoperative Management in Low-Grade Glioma Surgery within the European Low-Grade Glioma Network. 2010. Intraoperative electrical stimulation in awake craniotomy: methodological aspects of current practice. Neurosurg Focus. 28: E7.

Taylor RH, Stoianovici D. 2003. Medical robotics in computer-integrated surgery. Robotics and Automation, IEEE Transactions on. 19(5): 765-781.

Teulings HL, Contreras-Vidal JL, Stelmach GE, Adler CH. 1997. Parkinsonism reduces coordination of fingers, wrist, and arm in fine motor control. Exp Neurol. 146(1):159-170.

Tsetserukou D, Tadakuma R, Kajimoto H, Kawakani N, Tachi S. 2007. Intelligent variable joint impedance control and development of a new whole-sensitive anthropomorphic robot arm. In: Proc of IEEE Int. Symp. on computational intelligence in robotics and automation, 2007; p. 338–343.

Tsumugiwa T, Yokogawa R, Hara K. 2002. Variable impedance control based on estimation of human arm stiffness for human-robot cooperative calligraphic task. In Proc. of IEEE Int. Conf. on Robotics and Automation, 2002; p. 644–650.

Uneri A, Balicki MA, Handa J, Gehlbach P, Taylor RH, Iordachita I. 2010. New steady-hand eye robot with micro-force sensing for vitreoretinal surgery. In: Proc of IEEE Int Conf on Biomedical Robotics and Biomechatronics, 2010; p. 814-819.

Van Dommelen JAW, Hrapko M, Peters GWM. 2009. Mechanical properties of brain tissue: characterisation and constitutive modelling. In: Kamkin, A, Kiseleva, I, editors. Mechanosensitivity of the Nervous System. Springer Netherlands; p. 249-279.

Varma TRK, Eldridge P. 2006. Use of the NeuroMate stereotactic robot in a frameless mode for functional neurosurgery. Int J Med Robotics Comput Assist Surg. 2: 107–113.

Villani L, De Schutter J. 2008. Force Control. In: Siciliano B, Kathib O, editors. Handbook of Robotics. Springer; p. 161-185.

Wagner CR, Howe RD. 2007. Force feedback benefit depends on experience in multiple degree of freedom robotic surgery task. IEEE Trans. Robot. 23(6): 1235–1240.

Watson GA. 2006. Computing Helmert transformations. J COMPUT APPL MATH. 197(2): 387-394.

Wittek A, Kikinis R, Warfield SK, Miller K. 2005. Brain shift computation using a fully nonlinear biomechanical model. In: Medical Image Computing and Computer-Assisted Intervention–MICCAI 2005; p. 583-590.

Wittek A, Dutta-Roy T, Taylor Z, Horton A, Washio T, Chinzei K, Miller K. 2008. Subject-specific non-linear biomechanical model of needle insertion into brain. Computer methods in biomechanics and biomedical engineering. 11(2): 135-146.

Yamamoto T, Abolhassani N, Jung S, Okamura AM, Judkins TN. 2012. Augmented reality and haptic interfaces for robot-assisted surgery. Int J Med Robot Comp. 8(1): 45-56.

Yang C, Ganesh G, Haddadin S, Parusel S, Albu-Schaeffer A, Burdet E. 2011. Human like adaptation of force and impedance in stable and unstable interactions. IEEE T Robot. 27(5): 918–930.

Zanchettin AM, Bascetta L, Rocco P. 2013. Achieving humanlike motion: resolving redundancy for anthropomorphic industrial manipulators. Robotics and Automation Magazine. 20(4): 131-138.

Zeng G, Hemami A. 1997. An overview of robot force control, Robotica. 15(5): 473–482.

Zhang X, Zhang G, Yu T, Ni D, Cai L, Qiao L, Du W, Li Y. 2013. Surgical treatment for epilepsy involving language cortices: A combined process of electrical cortical stimulation mapping and intra-operative continuous language assessment. Seizure. 22(9): 780-786.